Reconstructing Arctic Sea Ice in the Common Era

Mary Kathleen Brennan

A thesis
submitted in partial fulfillment of the
requirements for the degree of

Master of Science

University of Washington

2019

Reading Committee:

Gregory Hakim, Chair

Cecilia Bitz

Eric Steig

Program Authorized to Offer Degree:
Atmospheric Sciences

University of Washington

Abstract

Reconstructing Arctic Sea Ice in the Common Era

Mary Kathleen Brennan

Chair of the Supervisory Committee:
Professor Gregory Hakim
Atmospheric Sciences

Arctic sea ice concentrations have undergone rapid declines in recent decades. Many factors have been shown to contribute to this decline, and much of it has been attributed to greenhouse gas forcing and natural variability. In order to understand the relative roles of these factors on Arctic sea ice decline, a longer record of spatially complete data is needed. This project employs data assimilation to combine climate model output and proxy records to reconstruct past climate fields using the Last Millennium Reanalysis (LMR) framework, resulting in spatially complete gridded fields with annual resolution over the last two millennia.

First the use of the LMR framework to reconstruct Arctic sea ice concentrations is tested through two methods: pseudo proxy experiments and comparing real proxy reconstructions to other records. Pseudo proxy results indicate strong performance in reconstructing Arctic sea ice. Correlation coefficients between the true and reconstructed values range between 0.63 and 0.77 depending on the climate model output used in the assimilation. The total Arctic sea ice extent reconstructed with the LMR using real proxy data compare well with satellite observations with correlation coefficients ranging between 0.54 and 0.84 depending on the climate model data used in the assimilation. These reconstructions were also compared to other records that precede satellite data and the LMR reconstructions show larger and longer lasting sea ice decline in response to early 20th century warming. The total sea ice

extent minimum observed in these reconstructions between 1920-1960 is similar to the values observed in the 1990s.

Next, two major questions are investigated using the 2000-year Arctic sea ice reconstruction: (1) Are the current sea ice changes unprecedented? and (2) Does sea ice respond to volcanic eruptions? The first is investigated through examining the distribution of total Arctic sea ice extent. The results indicate that both the trends and values of sea ice extent observed in the satellite era are unprecedented with respect to the LMR reconstruction of the last 1000 years. The second question is investigated through a composite average of sea ice extent before and after the 23 largest volcanic eruptions. These results show a statistically significant increase in total Arctic sea ice extent one year after an eruption.

Finally, the sensitivity of these reconstructions to proxy location, model prior and the number of prior ensemble members used in the data assimilation scheme is examined. These experiments indicate that the proxies in the Arctic region (above $60^{\circ}N$) explain most of the variance in the LMR sea ice reconstructions as expected. The role of the model prior is investigated by comparing the covariance between surface air temperature and Arctic sea ice across four different models. Overall the covariance is very similar except in some isolated regions in central Russia and China, in the North Atlantic and the central Pacific. In these regions the correlation coefficient is positive, but the coefficient of efficiency is negative indicating that there is a difference in the mean or variance in the covariance across models. 200 ensemble members are found to be sufficient in representing the variance in the full 1000 year last millennium model runs.

TABLE OF CONTENTS

LIST OF FIGURES

GLOSSARY

CCSM4: Earth system model developed at the National Center for Atmospheric Research

COEFFICIENT OF EFFICIENCY (CE): A measure of how overlapping two times series are as well as if there is a bias or differences in the variance (see mathematical definition in Section 2.2.9).

CORRELATION COEFFICIENT (R): A measure of how overlapping two datasets are (see mathematical definition in Section 2.2.9).

FORWARD MODEL: (H) In the Last Millennium Reanalysis framework this is a linear model converting a climate model to an equivalent proxy value. Also referred to as a proxy system model (PSM).

GISS: Global climate model developed at the Goddard Institute for Space Studies as part of the National Aeronautics and Space Administration.

HADCM3: Hadley Centre Coupled Model, version 3 - a global climate model developed at the Hadley Centre in the United Kingdom

LMR: Last Millennium Reanalysis

MPI: Global climate model developed at the Max-Planck-Institut for Meteorology

PRIOR: (x^b) The initial best guess of the climate state, with the Last Millennium Reanalysis framework this is a climate model output from a fully forced last millennium run

PRIOR ESTIMATE OF THE PROXY: (Hx^b) A prior value converted to a proxy value using a forward model

PROXY: A quantity that is measured retro-actively which gives information about some climate field in the past. Examples include ice cores, tree rings and corals.

PSEUDO PROXY: These are used as idealized observations in data assimilation. In this analysis, they are temperature values taken directly from a model (meaning no forward modeling is necessary) and are otherwise treated like proxy records in the assimilation process.

SEA ICE CONCENTRATION: The fraction of a grid cell covered by sea ice (%).

SEA ICE EXTENT: A binary fraction of a grid cell covered by sea ice (%) that takes the values 0% or 100% for a given cutoff percentage. For this analysis the sea ice concentration cutoff was 15%, so value less than or equal to 15% were set to 0%, and any concentration greater than 15% was set to 100%.

ACKNOWLEDGMENTS

The author wishes to express sincere appreciation to **Greg Hakim** for supporting her and her work, **Cecilia Bitz** for her willingness to meet and provide her sea ice expertise, and **Eric Steig** for his enthusiasm and encouragement throughout this project.

The author would also like to thank **Robert Tardif** for his help in building the infrastructure to perform these reconstructions, **Andre Perkins** for numerous helpful discussions related to python and the LMR and daily support as a stellar officemate, **Luke Parsons** for thoughtful discussions and encouragement, **Jessica Badgeley** for her support and thoughtful discussions related to the LMR and beyond, the rest of team Hakim **Dan Amrhein, Sara Sanchez, Gemma O'Connor, and Lindsey Taylor** for their support and feedback, **Noah Brenowitz** for his help with python and support as a stellar officemate, and **Edward Blanchard-Wigglesworth** for his expertise in sea ice. The author would also like to give **Abigail Swann** a special thanks for her mentoring and for standing up to make science more inclusive, and **Grads '16** for their comradery throughout graduate school.

The author wants to thank her family (**Mom, Dad, Bobby, Peyvand, Kiki** and **Ellis**) for their unwavering support and belief in me. The authors would also like to thank **Rosa, Sarah, Ty, Carolyn, Donna** and housemates (**Lian, Kate, Alex and Fannie**) for their pep talks particularly during the lows and their support as I confront and dissect gender and racial biases in the sciences and academia. I would not still be in science if it weren't for these radiant beings.

The author would also like to thank the National Science foundation for their support through the Graduate Research Fellowship Program, NOAA Award No. NA140AR4310176, and NSF Award No. AGS-1602223.

DEDICATION

to future generations who may not see sea ice in the Arctic

Chapter 1

INTRODUCTION

Arctic sea ice concentrations have undergone rapid declines in recent decades. Since the beginning of the satellite record in 1979, sea ice extent has exhibited a negative trend in all months with the largest negative values occurring in the last decade (Meier et al., 2014). These changes to sea ice coverage are exacerbated by corresponding changes to ice thickness, which has led to thinner, younger sea ice dominating the region. In the mid-1980s only about 35% of multiyear ice was relatively young (between 2 and 3 years old) while in 2007 this value rose to 58% (Maslanik et al., 2007). There are various feedbacks at play with Arctic sea ice, which makes it one of the most rapidly changing components of the climate system. Sea ice serves as an interface between the ocean and the atmosphere and large changes to this component of the climate system can have large impacts not only on local ecosystems and communities but also on the global climate system (Meier et al., 2014).

The two main factors contributing to this recent decline are thought to be greenhouse gas forcing and natural variability, but the overall effect is likely a combination of the two (Serreze et al., 2007). Some studies have shown that anthropogenic forcing is the main driver of the recent sea ice decline (Notz and Marotzke, 2012), but due to the short observational record, understanding the role of natural variability within this decline is difficult. Kay et al. (2011) used an ensemble of 20^{th} and 21^{st} century climate model runs to examine the relative role of anthropogenic forcing and natural variability on sea ice decline and found that natural variability explains about about half of the decline in September summer sea ice extent observations between 1979-2005. Having a better understanding of the natural variability is therefore crucial to our understanding of future sea ice change. Furthermore, understanding and quantifying the natural variability of sea ice would also help improve

model representation of these systems (Notz, 2015), which have been shown (in the ensemble mean) to deviate greatly from observations (Stroeve et al., 2007).

Short observational records make it hard to estimate the true natural variability of sea ice and also make it difficult to put the current declines in context. In order to gain a better understanding of natural variability, a temporally large and spatially comprehensive dataset is needed. One approach to obtain a longer record, is to look at sea ice of the past. Looking to pre-industrial time periods also isolates natural variability from greenhouse gas forcing. Here, data assimilation is implemented to produce an Arctic sea ice reconstruction spanning the last two millennia. This longer record will allow for the natural variability of sea ice to be investigated and the recent declines put in context.

Thus far, researchers have relied on three main types of data to study sea ice of the past: observations, proxy records and models. Below is a summary of some of previous work that's been done using these three types of data to build long-term records and reconstructions of sea ice.

1.1 Observational records

Observational records provide lower uncertainties than noisy proxy data, but their availability is sparse in both space and time. There are few records available before the satellite era and most of these point-wise observations were collected during the post-industrial period. Furthermore, in order to produce spatially complete data, interpolation of point-wise observations and other techniques is required. There are various regional and point-wise records available throughout the Arctic, but here the focus will be on the Walsh et al. (2017) record because it is the longest and most spatially complete observation-based record of Arctic sea ice to date.

For this record, the focus was to resolve the sea ice edge resulting in pan-Arctic sea ice extent values between 1850 to 2013. 14 different datasets from various sources were used ranging from satellite data, records from government agencies, and whaling and shipping records from across the Arctic. The different data sources were ranked based on data quality

(satellite being the highest rank) and the highest ranking data available for each region was used. The data between 1953 and 2002 was used to derive the relationship of sea ice concentration as a function of distance from the sea ice edge. For short time periods of missing data linear interpolation was used based on the data in preceding months. For longer periods of missing data, the average of the best analog years between 1953 and 2002 (based on the minimum root mean squared difference of ice concentrations over areas with data) was used. This is a valuable dataset that will be used for comparison in this analysis.

1.2 Model-based reconstructions

Climate models are powerful tools that have been used to model past and future climate as well as sea ice. Much of the focus in recent decades has been modeling current and future sea ice change. Often models are evaluated based on their agreement with observations, but anticipating recent declines has been notably difficult to model (Stroeve et al., 2007). Modeling past sea ice is particularly difficult given changes in the mean state and the limited number of sparse observations and proxy records available to verify the models back in time. Furthermore, Goosse et al. (2013) showed that nearly all models have a strong link between past and modern sea ice changes. Therefore understanding the biases and spread found in model results in the modern are necessary in order to improve past sea ice modeling. Much of the work to model the past climate has not included sea ice, and most of the studies that have have focused on modeling sea ice conditions during the Holocene (Renssen et al., 2005).

1.3 Proxy-based reconstructions

There are two general approaches to reconstructing Arctic sea ice with proxy records: using proxies that directly estimate sea ice conditions or using proxies that were developed as temperature-sensitive proxies (or other fields) and finding ways to relate that information to sea ice. A majority of the Arctic sea ice reconstructions to date have been regional reconstructions as opposed to pan-Arctic reconstructions. Below is a summary of some of the main studies that attempt to reconstruct sea ice with proxy data.

1.3.1 Sea ice sensitive proxies

Various sea ice proxies have been proposed in recent years. Their applicability for reconstructing pan-Arctic sea ice has yet to be demonstrated. Some proxies that have been proposed include: marine sediment cores, ice-rafted sediments, other marine organisms and chemical compounds, drift wood, whalebones, fossilized vegetation, and ice cores. These proxy records range from providing qualitative to quantitative information about sea ice conditions in a given region.

Examples of more qualitative measures include whalebones and driftwood. Whalebones are used to track the migration patterns of whales (for example the bowhead whale) which depend on the location of the sea ice edge. This information can give insights into summer sea ice conditions on millennial timescales (Dyke et al., 1996). The presence of different species of driftwood can indicate the presence or absence of land-fast ice given that logs are transported long distances by ice and are usually deposited on ice-free coastlines (England et al., 2008). These records are valuable in giving information about the large-scale changes to sea ice but lack ample temporal resolution to inform questions regarding higher frequency natural variability.

Two popular quantitative sea ice proxies that are under development are IP_{25} (Ice Proxy with 25 carbon atoms) in marine sediments and sea salt in ice cores. IP_{25} is a lipid and chemical biomarkers that was first proposed in Belt et al. (2007). The presence of this biomarker appears to represent seasonal sea ice conditions (Belt and Müller, 2013). Massé et al. (2008) used IP_{25} to reconstruct sea ice near Iceland over the last millennium and showed good correlation between reconstructed sea surface temperature and northern hemisphere temperature. Though useful in many regions near the sea ice edge, the applicability of these methods to the central Arctic where biological activity is low, still needs to be tested (Polyak et al., 2010). Sea salt in ice cores is another metric used as a sea ice indicator, but the relationship seems to have strong regional dependencies making it hard to generalize results (Polyak et al., 2010). Overall this is an exciting area of active research but the relationship

between these different compounds and sea ice is still not fully understood.

1.3.2 Temperature-sensitive proxies

Unlike sea ice-sensitive proxies, temperature-sensitive proxies have been under development for many decades. Many of these proxies are not just sensitive to temperature, and have been used to provide information about other climate variables (Cook et al., 2015). Given this precedence, there has been some work to utilize these records to reconstruct sea ice.

The most relevant reconstruction that used this approach is Kinnard et al. (2011). The authors used 69 terrestrial proxies to reconstruct summer Arctic sea ice coverage with 5 year resolution since 561 AD. They did this by calibrating their proxy network against historical observations of sea ice between 1979 and 1995 and then used partial least-squares regression to reconstruct sea ice back in time. Their method assumes that some portion of the variability in the proxy network is related to Arctic sea ice concentration and the relationship between proxies and sea ice is the same as in the calibration period through time. Their proxy database consists of circum-polar proxies that includes 52 ice cores, 11 tree rings, 4 lake sediments, and 2 historical sea ice observational records. They found that summer sea ice declines that began in the late 20^{th} century are unprecedented in both duration and magnitude compared to the variability observed in the rest of the 1,450 year reconstruction.

Using temperature sensitive proxies to reconstruct Arctic sea ice is a reasonable approach given that on longer timescales the relationship between annual mean Arctic sea ice area and annual mean global temperature is linear (Mahlstein and Knutti, 2012). Furthermore, there does not seem to be a tipping point or nonlinear effect for sea ice decline (Armour, K. C. and I. Eisenman and E. Blanchard−Wrigglesworth and K. E. McCusker and C. M. Bitz, 2011). Thus, using these more developed temperature-sensitive proxy records could be a promising approach for reconstructing sea ice, and this is the approach that will be utilized in this study.

1.4 Data assimilation reconstructions

Data assimilation is a technique that combines observations and model output to generate better estimates of climate fields. Different methods of data assimilation have been adapted to the paleoclimate realm so that proxy records can be combined with climate model output to reconstruct climate fields of the past.

Klein et al. (2014) used a particle filter data assimilation technique to reconstruct Arctic sea ice over a 400-year period in the mid-Holocene. This method involves running 96 climate model simulations with slightly different initial sea surface temperatures. After each time step (one year), each simulation is compared to a proxy-based reconstruction (which used dinocyst assemblages) and those that disagree (have a likelihood that's below a certain threshold) are abandoned. In order to maintain 96 simulations, the surviving states are resampled after each round of eliminations and a small error is added to the copied states before the simulation is run to the next time step. This method constrains the climate model to follow the proxy-based reconstruction, but does not directly incorporate information from the proxy records into the reconstruction. The resulting simulations show better agreement with proxy data, however large errors in the reconstructions remained due to low signal to noise ratios in the data.

Here we use an ensemble Kalman filter data assimilation method (discussed in Chapter 2) will be implemented using the Last Millennium Reanalysis (LMR) framework to reconstruct Arctic sea ice with annual resolution over the last two millennia. Singh et al. (2018) used an earlier version of the LMR to examine Atlantic multidecadal variability in the last two millennia and reconstructed Arctic sea ice to examine its response to Atlantic variability. They found that during a positive phase of the Atlantic Multidecadal Oscillation, sea ice thins over the Arctic and retreats over Greenland, Iceland, and Nordic seas. This work served as the basis and motivation for the work shown here, which aims to reconstruct Arctic sea ice in a more systematic manner with the LMR.

Chapter 2

METHODS

2.1 Paleoclimate Data Assimilation

Paleoclimate data assimilation is implemented to reconstruct Arctic sea ice over the past two millennia using the LMR framework. This framework is described in Hakim et al. (2016) and employs a square root ensemble Kalman filter as described in Whitaker and Hamill (2002). The goal of data assimilation is to objectively combine spatially complete model data with sparse point-wise observations in order to get a better estimate of climate fields.

Generally, data assimilation begins with a *prior* estimate, which is thought of as the initial 'best guess' of the climate state, and is updated by observations in regions where the two disagree. This technique allows point-wise observations to influence broader spatial regions based on spatial relationships derived from the prior. The prior and observations are weighted based on their relative uncertainty and the result are spatially complete gridded fields. The details of the square-root ensemble Kalman filter and its application in the LMR are described in this section as well as the experimental setup used to produce the reconstructions shown in this analysis.

2.1.1 A short primer on data assimilation

This section will serve as an introduction to the concepts of data assimilation. The details and implementation of these methods used for this study will be described in Section 2.1.3.

As mentioned above, data assimilation estimates a true unknown value (x) given a prior estimate (x^b) and observations (y). The following derivations, follow Chapter 13.6 in Holton and Hakim (2013). For the scalar case (one observation and one prior value), this can be expressed as the following equation

$$p(x^a) = p(x \,|\, y), \tag{2.1}$$

where x^a is the analysis, p represents the probability density function, and $p(x \,|\, y)$ represents the conditional probability density of x given y. Through Baye's Rule this can be transformed further so that

$$p(x^a) = p(x \,|\, y) = \frac{p(y \,|\, x)\, p(x)}{p(y)}. \tag{2.2}$$

The probability of the analysis is dependent on the flipped conditional probability, $p(y|x)$, which represents the likelihood of some observation, y, given x. In this case, $p(x)$ is the prior and $p(y)$ is simply a scaling constant and will be assumed to be 1. From here these likelihood functions are assumed to be normally distributed, which is a practical necessity when generalizing this to the case of multiple variables. With this assumption,

$$p(y \,|\, x) = c_1 e^{-\frac{1}{2}(\frac{y-x}{\sigma_y})^2} \tag{2.3}$$

$$p(x) = c_2 e^{-\frac{1}{2}(\frac{x-x^b}{\sigma_b})^2}, \tag{2.4}$$

where c_1 and c_2 are constants, x^b is the prior, σ_b^2 is the error variance of the prior and σ_y^2 is the error variance of the observation. Therefore,

$$p(x^a) = C e^{-\frac{1}{2}(\frac{x-x^b}{\sigma_b})^2} e^{-\frac{1}{2}(\frac{y-x}{\sigma_y})^2}. \tag{2.5}$$

There are different ways to solve this equation for x. Here we will take a minimum variance approach for which we define a cost function J:

$$J(x) = -log\,[\,p(x^a)] = \frac{1}{2}\frac{(x-x^b)^2}{\sigma_b^2} + \frac{1}{2}\frac{(y-x)^2}{\sigma_y^2} - log(C). \tag{2.6}$$

J represents the difference between the true value, x, and the prior and observation estimates respectively. In order to acquire the best fit, we want to minimize J. Doing so and solving for x and some algebraic manipulation leads to the update equation

$$x^a = x^b + \left(\frac{\sigma_b^2}{\sigma_b^2 + \sigma_y^2}\right)(y - x^b). \tag{2.7}$$

Given this equation, the error variance of the analysis (σ_a^2) is

$$\sigma_a^2 = \frac{\sigma_b^2}{1 + (\frac{\sigma_b}{\sigma_y})^2} = \frac{\sigma_y^2}{1 + (\frac{\sigma_y}{\cdot}\sigma_b)^2} < \sigma_y^2, \sigma_b^2 \tag{2.8}$$

This implies that the error variance of analysis is always less than that of the observations and prior, and therefore the mean analysis will have higher peak probability than either the prior or the observations. A visualization of this is shown in Figure 2.1 for a set of observations with a mean of 1.0 and variance of 0.25 and a set of priors with a mean of -1.0 and variance of 0.5. The resulting analysis has a mean of 0.33 and a variance of 0.17. In this example, there was more certainty in the observations (less variance) so the mean of the analysis resulting from the update equation is closer to that of the observations than that of the the prior. Also, the variance of the analysis in Figure 2.1 is less than the variance in both the observations and the prior. This indicates that the variance of the reconstruction (the analysis) is limited by the the variance in the observations and the prior.

All of these equations can be generalized to the multivariate case in which case x^a, x^b, and y become vectors, and σ_b^2 and σ_y^2 become error covariance matrices $\mathbf{B}$ and $\mathbf{R}$ respectively. $\mathbf{B}$ is the covariance matrix of the prior whose diagonal elements are the variance at each grid cell and the off diagonal elements is the covariance between different grid cells. $\mathbf{R}$ is the error covariance matrix of the observations and its a diagonal matrix and the diagonal elements are the error variance of each observation. For the multivariate case, update equation (see equation 2.7) becomes

$$\mathbf{x^a} = \mathbf{x^b} + \mathbf{K}(\mathbf{y} - \mathbf{H}\mathbf{x^b}), \tag{2.9}$$

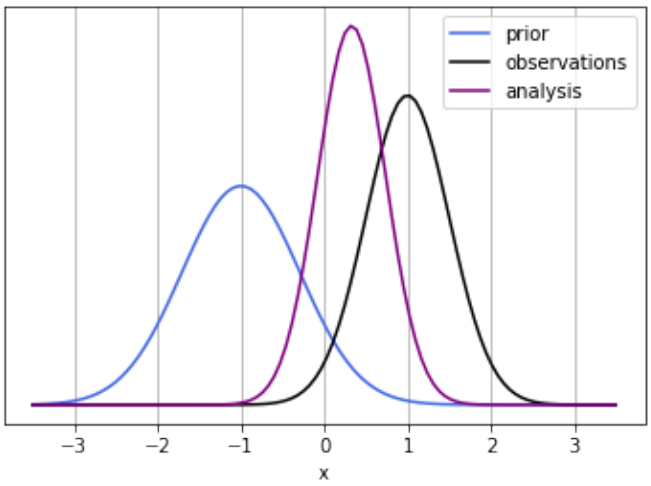

Figure 2.1: *The probability density function of the prior (blue), observations (black), and analysis (purple). The mean and variance of the prior are 1.0 and 0.5, 1.0 and 0.25 for the observations, and 0.33 and 0.17 for the analysis.*

where $\mathbf{B}$ is the error covariance matrix of the prior, $\mathbf{R}$ is the error covariance matrix of the observations ($\mathbf{y}$), $\mathbf{H}$ is a linear operator that converts the prior to observation space and $\mathbf{K}$ is the Kalman gain:

$$\mathbf{K} = \mathbf{B}\mathbf{H}^{\mathbf{T}}(\mathbf{H}\mathbf{B}\mathbf{H}^{\mathbf{T}} + \mathbf{R})^{-\mathbf{1}}. \tag{2.10}$$

In Equation 2.9, the difference between the observations ($\mathbf{x}$) and the prior estimate of the observation ($\mathbf{H}\mathbf{x}^{\mathbf{b}}$) is referred to as the *innovation*. In this form, it is clear that this technique is simply a weight of the innovation added to an initial best guess, or prior.

These equations are extremely powerful but often the dimensions of the covariance matrices, namely $\mathbf{B}$, are very large and expensive to calculate, so an approximation is necessary. For LMR framework, we adopt an ensemble approach, which uses a subsample of climate states from a model run to estimate $\mathbf{B}$. The specifics of the square-root ensemble Kalman filter technique used are described in the next section.

2.1.2 Square-root Ensemble Kalman Filter

A square-root ensemble Kalman filter approach with serial observations (Whitaker and Hamill, 2002) is employed in the LMR framework. For serial observations, only one observation is assimilated at a time. Thus the full covariance matrix ($\mathbf{B}$), which is usually extremely large, does not need to be calculated, just the covariance in the prior ensemble at one proxy location. With this approach an equation for the ensemble mean of $\mathbf{x^a}$ and the perturbations of $\mathbf{x^a}$ from its ensemble mean are solved separately:

$$\bar{\mathbf{x}}^{\mathbf{a}} = \bar{\mathbf{x}}^{\mathbf{b}} + \mathbf{K}(\bar{\mathbf{y}} - \mathbf{H}\bar{\mathbf{x}}^{\mathbf{b}}) \tag{2.11}$$

$$\mathbf{x'^a} = \mathbf{x'^b} + \tilde{\mathbf{K}}(\mathbf{y'} - \mathbf{H}\mathbf{x'^b}). \tag{2.12}$$

Here the overbars indicate the ensemble mean and the primes indicate the perturbations from the ensemble mean. $\tilde{\mathbf{K}}$ is an adjusted $\mathbf{K}$, gives the correct posterior covariance matrix. When a serial observation approach is used, each observation value is updated individually which simplifies the calculation. With this approach, $\tilde{\mathbf{K}} = \alpha\mathbf{K}$ and α is simply a constant

$$\alpha = \left(1 + \sqrt{\frac{\mathbf{R}}{\mathbf{HBH^T} + \mathbf{R}}}\right)^{-\mathbf{1}}. \tag{2.13}$$

2.1.3 Last Millennium Reanalysis Framework

For the LMR, the square-root ensemble Kalman filter is applied to reconstruct past climate. This involves assimilating sparse and noisy proxy data 'observations' into climate model output to reconstruct annual values.

In the LMR, the prior is a pre-existing fully forced last millennium climate model run. On longer timescales, in this case annual resolution, climate models have little predictive skill and are computationally expensive to run for 2000 years, so we adopt an offline approach (Oke et al., 2002; Evensen, 2003; Steiger et al., 2014). For offline data assimilation, the prior is a random sample of N_{ens} climate states (full global grid of a variable at a given year) drawn from a last millennium climate model run. N_{ens} random years are selected and those

climate states are used as the prior ensemble for every time step, resulting in a 2000-year reconstruction for each ensemble member. The ensemble size is chosen to be large enough so that the error covariance of the prior is a reasonable estimate of the error covariance of the entire climate model run (see Section 3.3.3). Since the ensemble is a random sample from a last millennium run, the prior estimate of the proxy will likely differ greatly from the proxy values, and therefore result in a large innovation. In these offline reconstructions, all the deviations from the ensemble mean are due to information coming from the proxies.

Proxy records are assimilated in the LMR as observations. 2,090 proxy records are used including: ice core, tree ring, lake sediment and coral records. All the records are sensitive to temperature while tree ring records are also sensitive to moisture or precipitation (the proxy database used will be discussed further in Section 2.2.1). When applying the equations from section 2.1.2 in the LMR, $\mathbf{H}$ is a linear forward model or proxy system model (PSM) to map the prior climate model data to an estimate of a proxy measurement. Each proxy record is fit to GISS surface temperature version 4 data (GISTEMP from Hansen et al. (2010)) between 1901-2000 CE. For tree ring data, a seasonal (determined objectively) fit with monthly Global Precipitation and Climatology Centre (GPCC) version 6 data (Schneider et al., 2014) and GISTEMP data was used as outlined in Tardif et al. (2019). Furthermore, the variance of the regression residuals derived from the PSMs is used at the error estimate of the observations, $\mathbf{R}$.

Despite the fact that none of the proxy records explicitly measure sea ice, this method can be used to reconstruct sea ice and other fields. To describe how sea ice variables are reconstructed, consider the update equation for a single proxy value:

$$\bar{\mathbf{x}}^a = \bar{\mathbf{x}}^b + \left(\frac{w_{loc} \circ cov(\mathbf{x}^b, \mathbf{H}\mathbf{x}^\mathbf{b})}{var(\mathbf{H}\mathbf{x}^\mathbf{b}) + \mathbf{r}}\right)(y - \mathbf{H}\bar{\mathbf{x}}^\mathbf{b}) \tag{2.14}$$

$$\mathbf{x}'^a = \mathbf{x}'^b + \left[1 + \sqrt{\frac{R_k}{var(\mathbf{H}\mathbf{x}^b) + R_k}}\right]^{-1}\left(\frac{w_{loc} \circ cov(\mathbf{x}^b, \mathbf{H}\mathbf{x}^\mathbf{b})}{var(\mathbf{H}\mathbf{x}^\mathbf{b}) + \mathbf{r}}\right)(\mathbf{H}\mathbf{x}'^\mathbf{b}). \tag{2.15}$$

Here, y is a single proxy observation and r is its error. w_{loc} is the covariance localization which cuts off the covariance at a certain distance from an observation and $\circ$ is the Schur product, or element-wise multiplication. Localization will be discussed further in Section 2.2.6. In the LMR framework, x^b is a large array containing both surface temperature and in this case sea ice concentration data for each ensemble member. $\mathbf{Hx^b}$ is the prior estimate of the proxy, so the innovation $(y - \mathbf{Hx^b})$ is in the unit of the proxy measurement. The Kalman gain determines the weight given to the innovation based on the relative uncertainty in the prior and proxy. The temperature information from the proxy records is related to sea ice concentration through the covariance between the sea ice concentration in the prior (at every grid cell) and the temperature at a proxy location in the prior converted to an equivalent proxy value via $\mathbf{H}$.

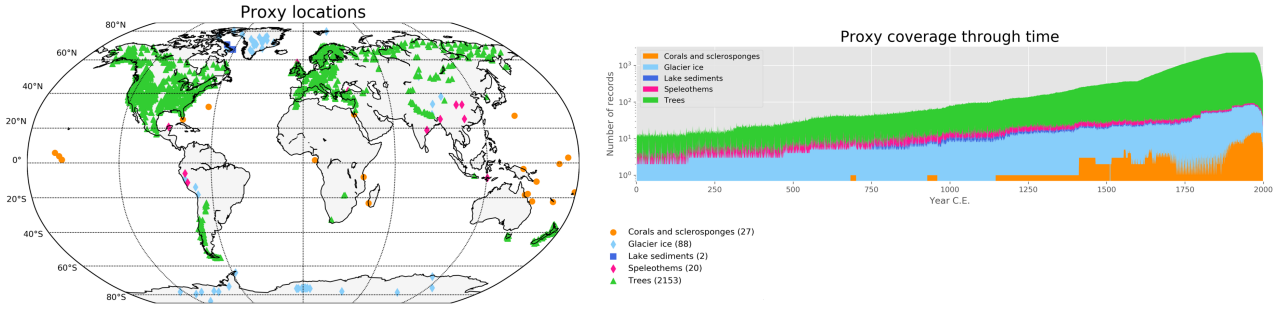

Figure 2.2: *The location of the proxy records in the LMRdbv1 database used (besides speleothems) for most of these reconstructions are shown as well as their temporal distribution.*

2.2 Experimental Setup

The following is a description of the specific LMR settings and parameters used to reconstruct Arctic sea ice.

2.2.1 Proxy Databases

Two proxy databases were assimilated in these reconstructions. The primary database used is outlined in Anderson et al. (2019) and will be referred to as LMRdbv1. Figure 2.2 shows a map of where the different records were collected and their number density through time. This dataset includes seven proxy types: corals and sclerosponges, bivalves, ice cores, lake sediments, marine sediments, speleothems and trees for a total of 2,794 records (speleothems were not used in these reconstructions). All these proxy records have at least annual resolution and all are sensitive to temperature and the trees are sensitive to both temperature and precipitation.

The second database used (only in Section 3.3.1) is from Pages2k Consortium (2013) and will be referred to as Pages2kv1. Figure 2.3 shows a map of where the different records were collected and their number density through time. This network includes considerably fewer records than LMRdbv1, with only 462 records.

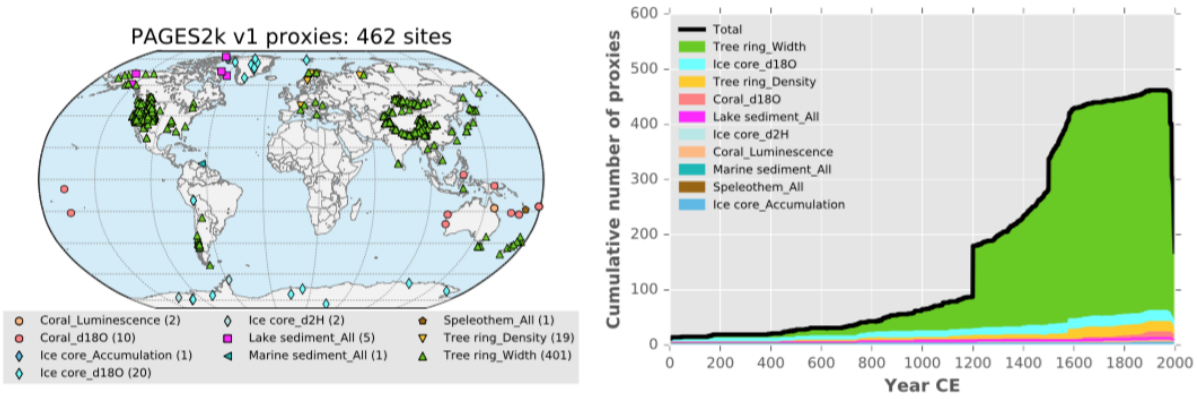

Figure 2.3: *The location of the proxy records in the Pages2kv1 network used (except for speleothems) in Section 3.3.1 as well as their temporal distribution.*

Some general observations include: tree records dominate these databases in quantity, a majority of the records were collected in the northern hemisphere, and most were collected on land though some ocean based records are included. Finally, there is a significant decrease

in proxy availability further back in time, in particular before around 1000 CE. At this time, the number of records drops below about 100.

2.2.2 Monte Carlo Iterations

Uncertainty in both the proxy error and the model covariance estimates, motivates the 5 Monte Carlo iterations performed for each reconstruction. For each of these iterations, 200 ensemble members are drawn from the model run and a random 25% of the proxy records are withheld for verification purposes. This allows us to subsample the uncertainty in the covariance in the prior ensemble as well as average over the error in the proxies. Subsampling also inhibits certain proxy records from dominating the reconstructions, as they may not be present in all iterations. The random draws are seeded so that the same years and proxies can be drawn for each iterations of reconstructions using different model priors. Results will show the average of all 1000 ensemble members (5 Monte Carlo iterations of 200 ensemble members each).

2.2.3 Variables Reconstructed

Here reconstructions of 2m air temperature and sea ice concentration are shown. Sea ice concentration is the percentage of a grid cell covered by sea ice. Some results will also be shown for total Arctic sea ice extent. Total sea ice extent is a measure of the area encompassed by the sea ice edge and is calculated from the reconstructed sea ice concentrations. For these calculations, if the concentration of a grid cell is greater than 15% it is said to have a sea ice extent of 100%, and if a grid cell has a concentration less than 15% than it is said to have a sea ice extent of 0%. All variables were reconstructed with annual resolution.

2.2.4 Priors

The LMR sea ice reconstructions rely on the covariance between temperature at each proxy location and Arctic sea ice concentration at every grid cell within the model prior (see

equations 2.2 and 2.6). The large scale structure of this covariance differs from model to model. To test the effects of these differences on the reconstructions, four different model runs: National Center for Atmospheric Research Community Climate System Model version 4 (CCSM4 (Landrum et al., 2013)), Max Planck Institute (MPI), NASA Goddard Institute for Space Studies (GISS), and Hadley Centre Coupled Model version 3 (Hadcm3) last millennium simulations were used. Each last millennium simulation was run between 850-1850 CE with full forcing as described in Schmidt et al. (2011). Gridded sea ice concentration data from each of these simulations was annually averaged and re-gridded to a standard 2° x 2° grid (the 20th Century Reanalysis grid as in Compo et al. (2011)) and used as priors.

2.2.5 Number of Ensemble Members

For these reconstructions, 200 ensemble members were used. The determination of this ensemble size is discussed in Section 3.3.3.

2.2.6 Localization

A pitfall of the Kalman gain is that spurious correlations can result from sample error in a finite ensemble (Hamill et al., 2001). Covariance localization is a technique used to reduce such affects by cutting off the covariance pattern at a certain distance from the location of an observation. In the LMR framework, a Gaspari-Cohn fifth-order polynomial is used (Gaspari and Cohn, 1999). For this method, the covariance localization is a distance-weighted filter, w_{loc}, on the prior covariance (through the Schur product, or element-wise multiplication, denoted by $\circ$) as shown in equations 2.14 and 2.15. All LMR reconstructions shown here, used a localization radii of 25,000 km is used.

2.2.7 Percentage Cutoff

As mentioned in section 2.1.1, the likelihood function of the analysis is assumed to follow a Gaussian distribution. Sea ice concentration however, does not necessarily follow a Gaussian

distribution since in most regions either 0% or 100% are the most likely. If there is sea ice present in a given grid cell in any of the ensemble members, the Kalman filter approach will result in sea ice variability at that grid cell for all times. Therefore, the analysis can result in values greater than 100% and less than 0%. When this occurs, the values at each grid cell and time for each ensemble member were cutoff at 0% and 100% before taking an ensemble mean. Sea ice concentration anomalies (centered about 1979-2000) were reconstructed using the LMR so first the mean sea ice concentration from satellite data (Fetterer et al., 2017) was added to the reconstructed anomalies and then the percentages were cutoff.

2.2.8 Total Arctic sea ice extent calculations

The total Arctic sea ice extent is often used here to represent the pan-Arctic sea ice conditions. Sea ice concentration was reconstructed by the LMR and the total sea ice extent was calculated after the reconstruction was complete. Sea ice extent is defined as the 15% cutoff of sea ice concentration. Thus, if the concentration is less than 15%, the extent is set to zero, and if the concentrations is greater than 15%, the extent is set to be 100%. The total Arctic sea ice extent is simply the sum of the sea ice extent at each grid cell in the northern hemisphere, and can be thought of as the area encompassed by the sea ice edge. Both ocean fraction and area of each grid cell were taken into account in these calculations.

2.2.9 Verification Statistics

The correlation coefficient and coefficient of efficiency are used to evaluate the performance of these reconstruction.

Correlation Coefficient

The correlation coefficient measures how in phase two time series or spatial patterns are. Though an important metric, the correlation coefficient does not account for differences in amplitude or biases between to datasets. It is bounded between -1.0 and 1.0. It is defined

as:

$$r = \frac{\sum_{i=1}^{n}(x_i - \bar{x})(v_i - \bar{v})}{\sqrt{\sum_i^n (x_i - \bar{x})^2}\sqrt{\sum_i^n (v_i - \bar{v})^2}} = \frac{cov(x, v)}{\sigma_x \sigma_v}. \tag{2.16}$$

Coefficient of Efficiency

The coefficient of efficiency (CE), like the correlation coefficient, measures how closely two datasets overlap, but also if there is a bias or difference in variance between the two datasets. This is a much harder metric to perform well at. Its maximum value is 1.0 and it is unbounded in the negative direction. A CE value of zero is when the sum of squared errors is equal to the variance in the verification data. Generally, the goal is to obtain positive CE values. It is defined as:

$$CE = 1 - \frac{\sum_i^n (v_i - x_i)^2}{\sum_i^n (v_i - \bar{v})^2}. \tag{2.17}$$

Here v is the verification value and x is the value being evaluated (often the reconstructed value).

Chapter 3

RESULTS

3.1 Pseudo Proxy Experiments

Pseudo-proxy experiments are an idealized framework where temperature values from model output are used as observations in the LMR. In previous studies, pseudo proxy experiments have been used to test the validity of the LMR reconstructions of surface temperature (Steiger et al., 2014). Here the focus is to evaluate the LMR's performance in reconstructing Arctic sea ice. In these experiments the pseudo proxies are given low random error and are therefore heavily weighted in the Kalman filter, which implies that these results an upper bound on LMR performance.

3.1.1 Perfect model pseudo proxy experiments

Perfect model pseudo proxy experiments draw both the prior ensemble and pseudo proxy observations (temperature values) from the CCSM4 last millennium run. The locations of pseudo proxy observations are the real proxy locations from the LMRdbv1 database, and the same locations are used each year. Pseudo proxy values are the 2m air temperatures at the nearest grid cell to each real proxy location in the CCSM4 last millennium run. For these experiments, the sea ice concentration values in the CCSM4 last millennium run are the *true* values and we know that the covariance structure between temperature and sea ice in the prior ensemble is correct.

The 2,411 pseudo proxy observations were assigned an error of a random number drawn from a normal distribution with a variance of 0.1. In the real proxy database, the number of proxy records is far from constant in time, so using a large number of proxies at each time step results in an upper bound on LMR performance. The 600 year period, between

1250-1850, is reconstructed.

First, total Arctic sea ice extent is considered to evaluate the LMR sea ice reconstructions. Figure 3.1 shows the total reconstructed annual Arctic sea ice extent (in cyan) and that from the CCSM4 last millennium run (in black). The verification statistics are shown in Table 3.1. Overall the LMR is able to capture the multi-decadal variability of total Arctic sea ice extent well, and some of the the inter-annual variability and extremes (see Figure 3.1).

	Correlation coefficient	Coefficient of Efficiency
Unfiltered	0.77	0.51
30-year lowpass filtered	0.98	0.82

Table 3.1: *The correlation coefficient and coefficient of efficiency between the total annual Arctic sea ice extent from the CCSM4 last millennium run and the LMR reconstructed values using pseudo proxies from the same model output.*

Next, the performance of the LMR is evaluated spatially at each grid cell. The correlation coefficient and CE between the true the reconstructed annual sea ice extent anomalies between 1250-1850 at each grid cell is shown in Figure 3.2. Only correlation coefficients that pass a t-test at the 95% confidence level are shown.

Overall there is positive correlation between the true and reconstructed sea ice concentration anomalies everywhere in the Arctic. The correlation coefficients are greatest in coastal regions around Alaska, Hudson Bay, Iceland, Kamhatka Peninsula, in the Gulf of Bothnia between Finland and Sweden, and in the Barents Sea, exceeding 0.6 in all of these regions. This indicates that in these regions near the sea ice edge the timing of sea ice variability is well captured. The CE also shows positive values in the same regions with slightly negative values in the central Arctic, the Canadian Archipelago, and in some regions of the north Atlantic and Pacific. These positive values indicate that not only the timing of sea ice variability is well represented, but also the mean and variance.

The negative CE values are likely due to the fact that sea ice concentration data is

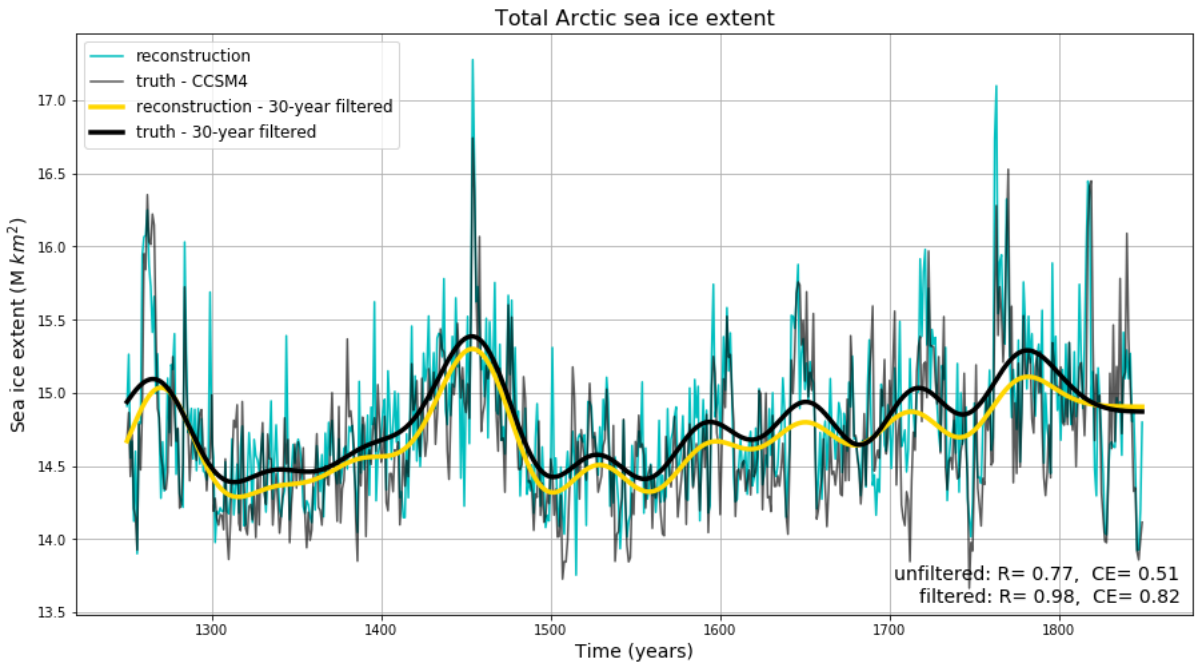

Figure 3.1: *The total annual Arctic sea ice extent (north of* $60°N$*) from the CCSM4 last millennium run (black) and reconstructed with the LMR (cyan) using pseudo proxies from MPI last millennium run. The 30-year lowpass filtered data is also shown in black and yellow respectively.*

non-Gaussian, meaning the most likely values tend to be zero or 100% coverage in some locations. In both of these regimes, the sea ice concentrations tend to be fairly constant. Reconstructing this is difficult because if there is sea ice at these grid cells in any one of the ensemble members, the LMR will reconstruct sea ice variability at all times about the ensemble mean. Therefore, the LMR tends to overestimate the variance in regions in the central Arctic where the sea ice concentration is stable around 100% and near the sea ice edge where there is mostly no sea ice in a given year, which is where there is negative CE in Figure 3.2. Some isolated grid cells have very negative CE values, in particular in the North Atlantic region and in the North and Baltic seas where there mostly no sea ice with some isolated years of sea ice presence. Figure 3.5 shows an example of such a grid cell, and this will be discussed further in Section 3.1.2.

Higher correlation coefficients and CE values do occur in near regions where there is high

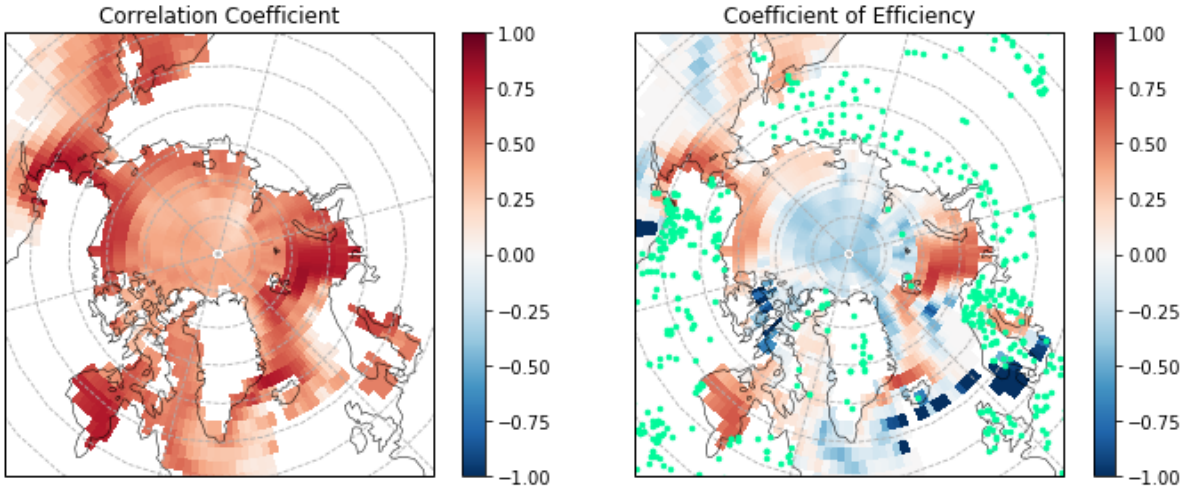

Figure 3.2: *The correlation coefficient and coefficient of efficiency for sea ice concentration anomalies is shown for pseudo-proxy experiments using CCSM4 last millennium run as the prior and temperature pseudo observations. The years 1250-1850 were reconstructed, and 2,411 proxy locations were used and are shown in mint green on the right.*

proxy density. However, northern and southern Greenland or north of central Russia have high proxy density, but show low correlation coefficient and negative CE values. Generally, the LMR is able to capture the total Arctic sea ice extent as well as the spatial variability at the sea ice edge within this idealized framework.

3.1.2 Imperfect pseudo proxy experiments

For *imperfect* pseudo proxy experiments, the prior ensemble is drawn from the CCSM4 last millennium run and the pseudo proxy observations (temperature values) are drawn from the MPI past 1000 run. The goal is to reconstruct sea ice from the MPI last 1000 run, given temperature output from the same run at sparse geographical locations and the spatial covariance structure from a different model run (CCSM4 last millennium run). As in real proxy experiments (see Section 3.2), with imperfect pseudo proxy experiments we know that the covariance structure between temperature and sea ice in the prior ensemble is incorrect (its derived from a different model than the true values). Therefore, these experiments will

indicate how dependent the reconstructions are on the prior and give a much more realistic performance bound on the LMR sea ice reconstructions.

For these experiments, as with the perfect model pseudo proxy experiments, the 600 year period between 1250-1850 CE is reconstructed using the same 2,411 pseudo proxy locations (derived from the LMRdbv1 database) each year.

The total reconstructed annual Arctic sea ice extent is used to evaluate the overall performance of these reconstructions. The results are shown in Figure 3.3 with total reconstructed annual Arctic sea ice extent in cyan and the true value from the MPI last millennium run in black.

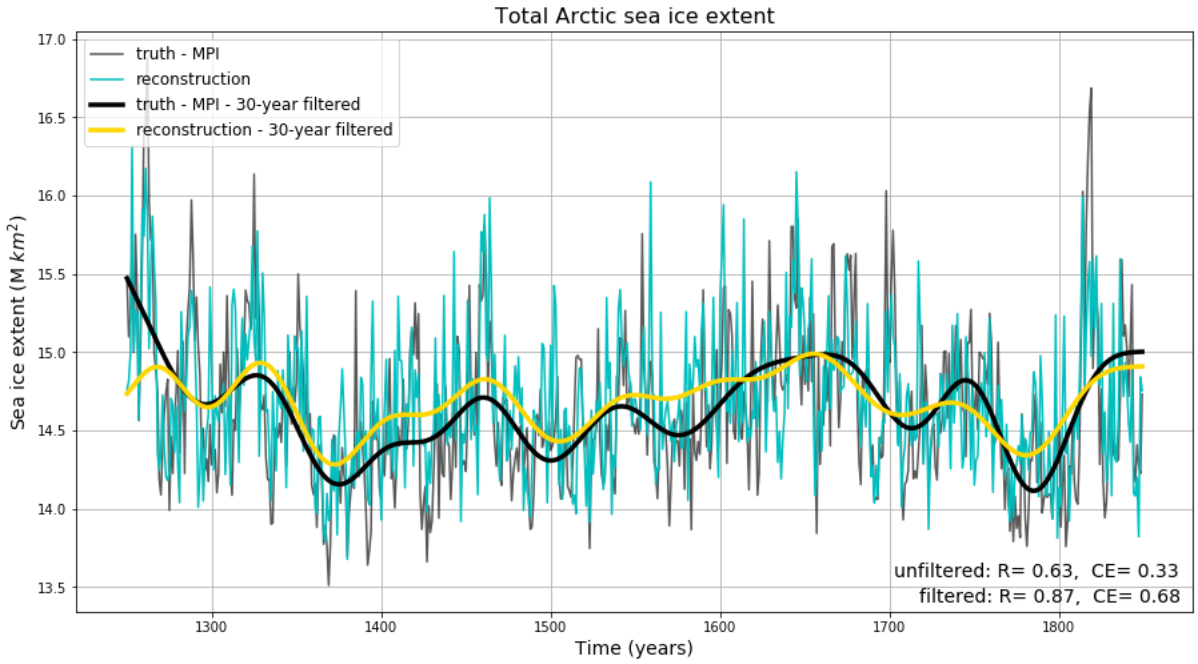

Figure 3.3: *The total Arctic sea ice extent (north of* $60°N$*) from the MPI past 1000 run (black), and the reconstructed values with the LMR (cyan) using pseudo proxies from MPI and CCSM4 as the prior. The 30-year lowpass filtered data is also shown in black and yellow respectively.*

As expected, these LMR reconstructions shows slightly weaker performance for the imperfect experiments. The verification statistics are shown in Table 3.2. Despite slightly weaker performance than perfect model pseudo proxy experiments, these imperfect experi-

ments still capture the multi-decadal and some of the inter-annual variability of total Arctic sea ice extent.

	Correlation coefficient	Coefficient of Efficiency
Unfiltered	0.63	0.33
30-year lowpass filtered	0.87	0.68

Table 3.2: *The correlation coefficient and coefficient of efficiency between the total annual Arctic sea ice extent from the true and reconstructed values. The true values are derived from the MPI last 1000 run and the LMR reconstructed values from imperfect pseudo proxy experiments which using a prior ensemble drawn from the CCSM4 last millennium run and the pseudo proxy observations drawn from the MPI last 1000 run.*

Next, the spatial performance of the imperfect pseudo proxy reconstructions is evaluated. Figure 3.4 shows the correlation coefficient and CE values at each grid cell between the reconstructed sea ice concentration anomalies with the true values (MPI past 1000 run) in color. There is positive correlation in most of the Arctic, though slightly weaker magnitude than the results from perfect model pseudo proxy experiments from section 3.1.1 (see Figure 3.2). Like in the perfect pseudo proxy experiments, there is positive CE values in regions where there is high correlation, but overall there are larger regions of negative CE, many of which are near the sea ice edge.

To investigate these negative CE values further, Figure 3.5 shows the time series at one grid cell near the Fram Strait which exhibits very negative CE values. The true time series (black line) at this location indicates that there was no sea ice variability most years (thus no sea ice), with some isolated years of sea ice coverage. As mentioned previously, when sea ice is present in any of the prior ensemble members, then the LMR reconstructed ensemble mean that show sea ice variability in all years. Individual grid cells in the Bering sea were also looked at and the time series look very similar to Figure 3.5. Other regions that exhibit negative CE, but are not necessarily near the sea ice edge include regions north of Alaska and in Baffin Bay. In both of these regions, the LMR reconstructions overestimate the variance of sea ice concentration anomalies, and it is still unclear why this is happening in these regions.

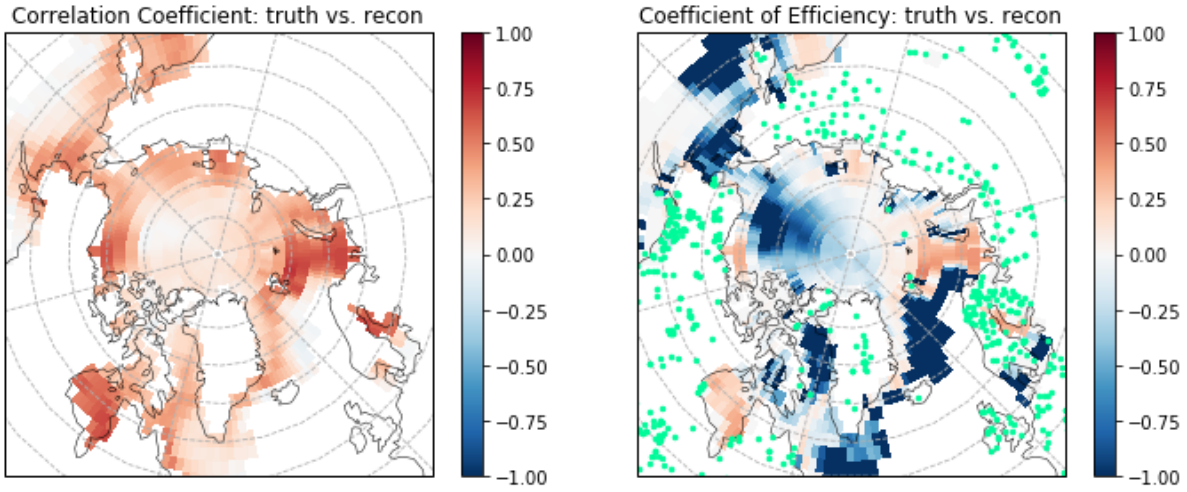

Figure 3.4: *The results of imperfect pseudo proxy experiments where the prior ensemble was drawn from the CCSM4 last millennium run and the pseudo proxy 'observations' were drawn from the MPI past 1000 run. The correlation coefficient and coefficient of efficiency for sea ice concentration anomalies is shown between the reconstruction and the true values (MPI). The years 1250-1850 were reconstructed, and the same 2,411 pseudo proxy locations were used for every year.*

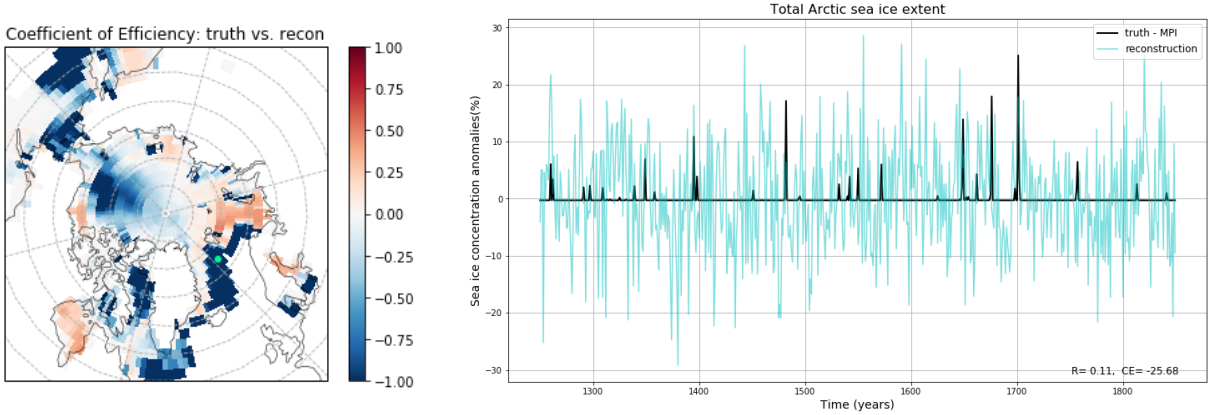

Figure 3.5: *On the left is the CE values between the true and reconstructed sea ice concentration values. On the right is the time series of a single grid cell near the Fram Strait (shown in mint green on the map on the left) of the true (MPI past 1000 run) and reconstructed sea ice concentrations.*

As a whole, the LMR reconstructions from imperfect pseudo proxy experiments show slightly weaker performance than the perfect model pseudo proxy experiments, but still perform well within this more realistic framework. This indicates that the prior has some

influence on the reconstruction likely through the inherited covariance structures from the prior ensemble.

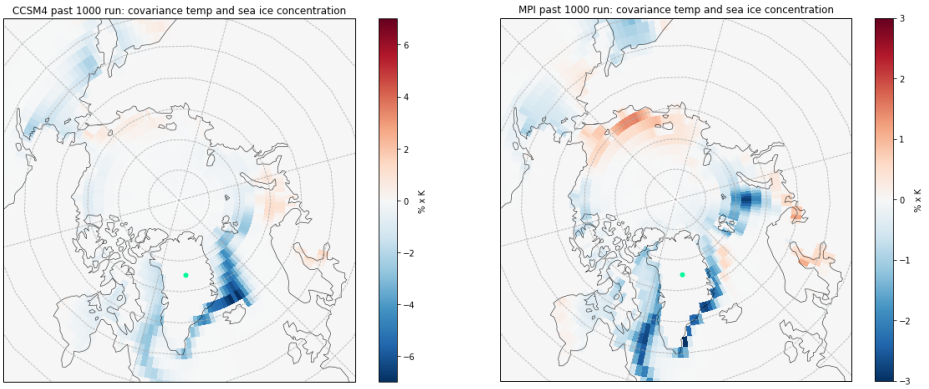

Figure 3.6: *Covariance of temperature at a point in Greenland (shown in cyan) and sea ice concentration everywhere for the MPI past 1000 run (right) and the CCSM4 last millennium run (left).*

The covariance structures between temperature and sea ice in the prior ensemble influences the weight and spatial reach of the innovation. These covariance structures and their magnitudes vary between different models making it difficult to reconstruct one model (or real sea ice values) using another. Figure 3.6 shows the covariance between the temperature at one grid cell in Greenland (a proxy location) and Arctic sea ice concentration everywhere from the CCSM4 and MPI last millennium runs. The patterns in Figure 3.6 differ in both their spatial distribution and magnitude which means that the information at this proxy location in Greenland is weighted and spread differently by the Kalman filter depending on which prior is used. Differences in covariance patterns exist across models at other proxy locations as well. How similar these covariance patterns are across four different models will be explored further in Section 3.3.

Also, the mean state and location of the sea ice edge differ across models. Figure 3.8 shows the mean anomalies from the CCSM4 and MPI last millennium runs as well as the differences between the two. These differences could also contribute to difficulties in reconstructing sea ice output from one model using a prior ensemble drawn from different model output.

In general both the perfect and imperfect pseudo proxy experiments show that the LMR

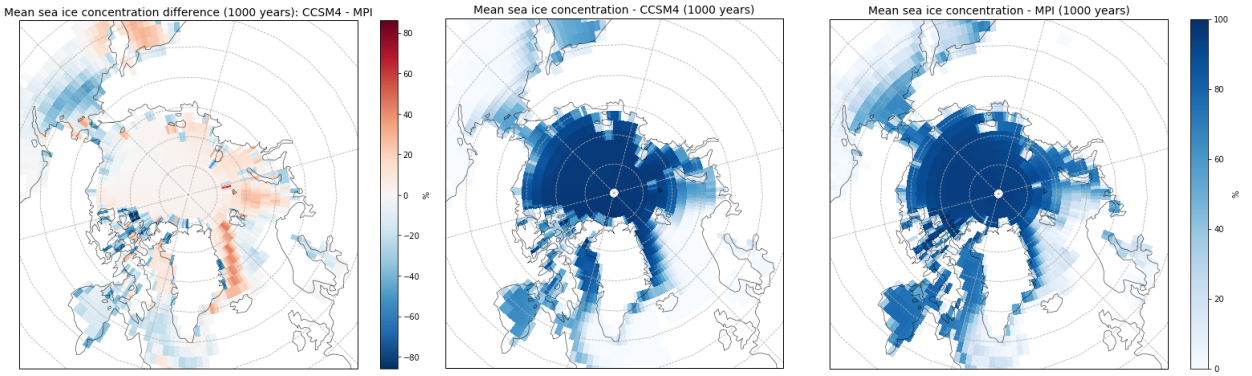

a) b) c)

Figure 3.8: *Shown are the 1000 year mean sea ice concentrations from the CCSM4 (b) and MPI (c) last millennium runs. The difference between the two is shown in panel (a).*

is a useful framework for reconstructing Arctic sea ice on annual timescales.

3.2 Real Proxy Reconstructions

Real proxy data is assimilated into climate model output in order to reconstruct sea ice conditions over the last two millennia. The LMR sea ice reconstructions are compared to other observationally based and proxy reconstructions to further test their performance. Then, the full 2000 year reconstructions are used to investigate whether the current sea ice changes observed in the satellite record are unprecedented and whether Arctic sea ice responds to volcanic eruptions.

3.2.1 Comparison to other records

For the following comparisons, prior ensembles were drawn from four different last millennium runs: CCSM4, Hadcm3, MPI, and GISS. Different model priors were used in order to test how dependent the results were on the prior.

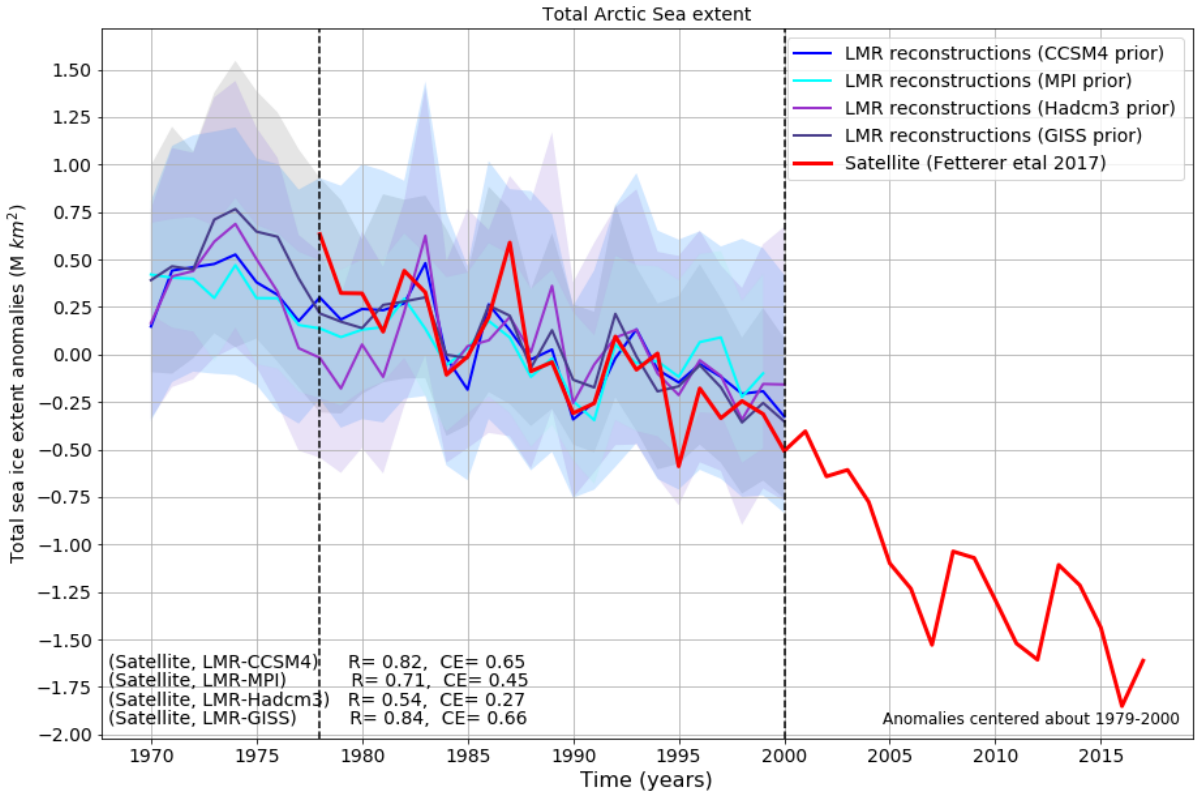

Figure 3.9: *Comparison of total Arctic sea ice extent from four LMR reconstructions stemming from four different priors (CCSM4, Hadcm3, MPI, and GISS) and satellite data from Fetterer et al. (2017). In the left corner the correlation coefficients and coefficients of efficiency between each reconstruction and the satellite data are shown. The shading indicates the* 95^{th} *and* 5^{th} *percentiles from all the ensemble members (5 Monte Carlo iterations of 200 ensemble members each).*

Satellite Comparison

The total reconstructed annual Arctic sea ice extent derived four different model priors (CCSM4, MPI, Hadcm3, and GISS) are compared satellite data in Figure 3.9. The LMR reconstructed time series shown are the ensemble mean over 5 Monte Carlo iterations with 200 ensemble members each. The total Arctic sea ice extent index from satellite data was taken from Fetterer et al. (2017), and all the results shown are anomalies centered about 1979-2000 CE. The LMR reconstructions shown in Figure 3.9 compare well with the satellite data and also show good agreement with one another. The CCSM4 prior LMR reconstruction

shows the best comparison with satellite data, with a correlation coefficient of 0.82 and a CE value of 0.65. The satellite data compares worst with the Hadcm3 past 1000 run prior LMR reconstruction, with a correlation coefficient of 0.54 and a CE values of 0.27. Generally, the satellite data falls within the 5th and 95th percentile of the ensemble spread (shading in Figure 3.9) for all four reconstructions. However, the reconstructions underestimate both of the trend and variability during the satellite era as shown in Table 3.3

Data source	Trends ($10^4 km^2/year$)	Variance ($(10^4 km^2/year)^2$)
Satellite	-3.8	9.8
MPI LMR reconstruction	-1.3	2.3
Hadcm3 LMR reconstruction		4.6
GISS LMR reconstruction	-2.6	

Table 3.3: *The trend and variance in the satellite data between 1979-2000 CE as well as the maximum and minimum trends and variances from the four LMR reconstructions. All trends were calculated using a linear fit.*

Walsh et al 2017 Comparison

Next, the LMR reconstructions are compared to the Walsh et al. (2017) dataset. As described in Section 1.1, this dataset combined various observational records, resulting in a gridded Arctic sea ice extent record from 1850-2000. The Walsh et al. (2017) record is shown as a black bold line in Figure 3.10, and the satellite data used for the previous comparison (Figure 3.9) is shown in red. In the later periods of the dataset, Walsh et al. (2017) relied on satellite data, which explains why these two datasets align so closely. Figure 3.10 also includes four LMR reconstructions derived from four different model priors (CCSM4, Hadcm3, MPI, and GISS). Shown is the ensemble mean over 5 Monte Carlo iterations with 200 ensemble members each all anomalies are centered about 1979-2000 CE.

The LMR reconstructions generally agree with the Walsh et al. (2017) record after around

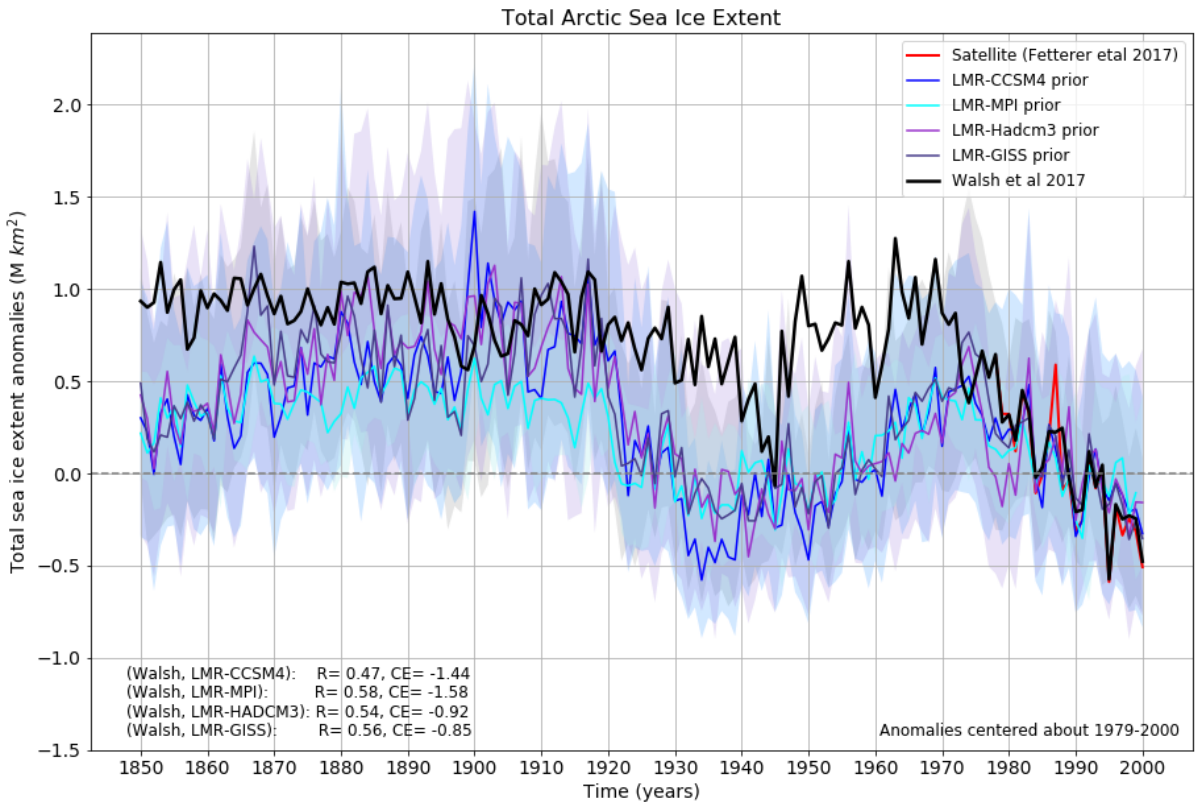

Figure 3.10: *Comparison of total Arctic sea ice extent from four LMR reconstructions stemming from four different priors (CCSM4, Hadcm3, MPI, and GISS) and that from Walsh et al. (2017). Anomalies are centered about 1979-2000. In the right corner the correlation coefficients and coefficient of efficiencies between each reconstruction and the Walsh dataset are shown. Each of the LMR ensemble means showed used 200 ensemble members and 5 Monte Carlo iterations.*

1975 CE and between around 1875-1920 CE, but diverge in the early portion of the record and in the early 20^{th} century, between 1920-1970 CE. The correlation coefficient of total Arctic sea ice extent in the reconstructions and the Walsh et al. (2017) record range between 0.47 (CCSM4 prior) and 0.58 (MPI prior), and the CE values range between -0.85 (GISS prior) and -1.58 (MPI prior). The LMR reconstructions and Walsh et al. (2017) diverge the most in the early 20th century. Between 1940-1945 CE, the Walsh et al. (2017) record shows an isolated period of low Arctic sea ice extent similar to that of the 1980s. All four LMR reconstructions show a much longer period of low sea ice conditions, lasting from around

1920 to 1970 CE, to levels observed in the 1990s.

Early 20th century warming in the high northern latitudes has been well documented (Yamanouchi, 2011) and is thought to be similar to the warming experienced between 1980-2010 CE. This warming was isolated to the northern hemisphere and some studies indicate that the warming was more pronounced in the Atlantic sector of the Arctic (Overland et al., 2011). According to Yamanouchi (2011), because the signal is not observed in the global mean indicates that a single external forcing is not a likely cause, and it was most likely some combination of natural variability and positive feedbacks that amplified atmospheric and radiative forcing. Figure 3.11 shows the zonal mean surface air temperature anomalies from an LMR reconstruction (CCSM4 prior) separated into three latitude ranges and a similar results from observations (figure taken from Yamanouchi (2011) (Figure 5)). In both the reconstructions and observations the anomalies are greatest at higher latitudes with anomalies exceeding $1°C$ (dark blue lines in Figure 3.11) but are not observed in the global mean temperature (black line in Figure 3.11). This period of warming started in the early 1920s and lasted until around 1940 CE, followed by about 20-30 years of cooling.

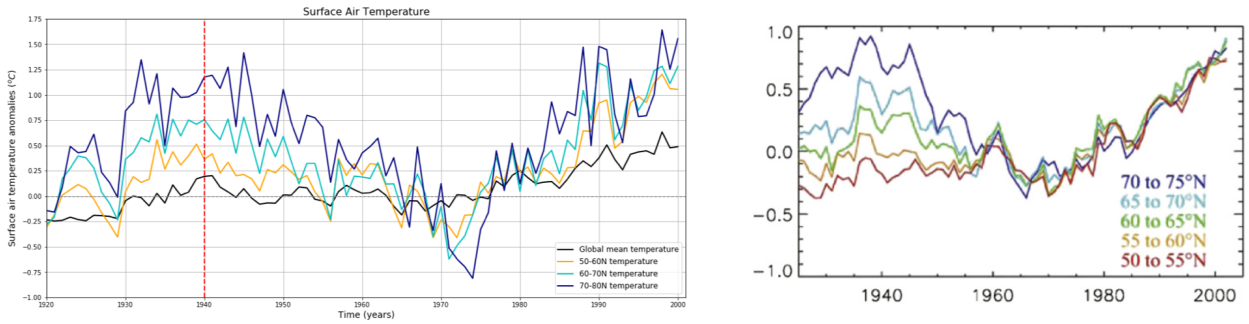

Figure 3.11: *At the left are LMR ensemble mean surface air temperature reconstructions using CCSM4 as the prior, 200 ensemble members, and 5 monte carlo iterations. The global mean in shown in black and the colored lines show the zonal mean of three different latitude ranges. Anomalies are centered about 1960-1980. The vertical red dashed line simply highlights the year 1940 which is near the inflection point of the anomalous warming. The figure at the right is Figure 5 from Yamanouchi (2011) and shows similar results from observations which were taken from Jones and Moberg (2003).*

Other studies have shown a decline in sea ice extent in response to early 20th century warming was isolated to certain regions of the Arctic. Polyakov et al. (2003) used observa-

tional records to investigate sea ice extent between 1900-2000 CE in four different seas north of Russia: Kara, Laptev, East Siberian, and Chukchi Seas. In three of these seas (Laptev, East Siberian, and Chukchi Seas) the sea ice extent has little to no anomaly around 1940 CE (see Figure 2 in Polyakov et al. (2003)). However, in the Kara sea, there is a large negative sea ice extent anomaly between around 1935-1960 CE, which is consistent with the LMR reconstructions in Figure 3.10. Out of the four seas examined in Polyakov et al. (2003), the Kara sea is that closest to the north Atlantic. The similarities of these observational records in this region to the LMR reconstructions indicate that the reconstructions may be dominated by the variability observed in the Atlantic sector. This is reasonable given that the strongest covariance between temperature and sea ice in the models tends to be in the North Atlantic.

Overall the period of early 20th century warming is well represented in the LMR reconstructions of surface air temperature when compared to the observations. The LMR framework indicates this anomalously warm period led to a pronounced period of low sea ice extent with levels similar to that observed in the 1990s. Further investigation is necessary to determine whether the sea ice extent levels between 1920-1970 CE shown in Walsh et al. (2017) or the LMR results shown here are more likely.

Kinnard et al 2011 Comparison

Kinnard et al. (2011) used a proxy database and partial least-squares regression (discussed in Section 1.3.2) to reconstructed summer sea ice extent. The LMR reconstructions shown here are all annual resolution so a direct quantitative comparison between the LMR and Kinnard et al. (2011) reconstructions is not possible, so we will rely on a qualitative comparison.

Figure 3.12 shows the two reconstructions of total sea ice extent on the same plot and the first difference to note is that the LMR reconstruction exhibits much less variability on the longer timescales than the Kinnard et al. (2011) reconstruction. It is expected that the annual reconstructions would show less variability than a summer sea ice reconstruction, though this may not account for the full differences in variability exhibited. Recent work

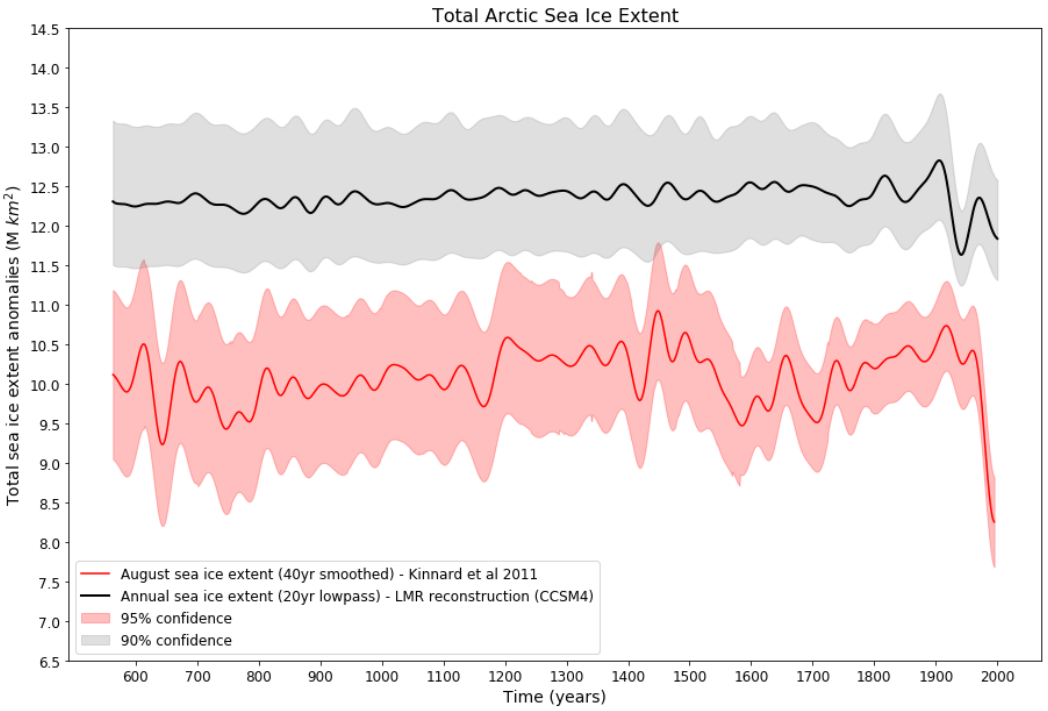

Figure 3.12: *Shown in black is an LMR reconstruction of total Arctic sea ice extent using CCSM4 as the prior (200 ensemble members and 5 iterations) with a 20 year low pass Butterworth filter applied. In red, is the summer sea ice extent reconstructed in Kinnard et al. (2011). The shaded regions indicate the 90th and 95th confidence intervals respectively.*

indicates that some of this damped variability might be due to some of the tree ring proxy records in the LMRdbv1 database. In order to investigate this further, reconstructions without these proxies need to be done.

Another noteworthy difference between these two reconstructions is that though both reconstructions show a similar pattern of variability in the 1900s, the LMR reconstruction shows a much larger magnitude of this variability. Kinnard et al. (2011) note a period of elevated sea ice between 1200-1450 CE and 1800-1920 CE, but these time periods do not stand out in the LMR reconstructions. Both reconstructions do indicate that the current declines starting in the late 20th century are unprecedented in duration and magnitude compared to the rest of each reconstruction.

3.2.2 2000-year sea ice reconstructions

The full 2000-year reconstruction of total Arctic sea ice extent, derived using a prior drawn from the CCSM4 last millennium run, is shown in Figure 3.13. Shown is the ensemble mean of 5 Monte Carlo iterations with 200 ensemble members each. First note that since the prior is constant in time, the ensemble mean of the prior is a flat line through time. All the deviations from a flat line in the LMR reconstructions are due to information from proxy records. The number of proxy records significantly increases with time; therefore, so does the variance of the reconstructions. The 5th and 95th percentile of the ensemble spread (shown as grey shading in Figure 3.13) also increases (larger spread) further back in time. Thus, the variance in our reconstructions is dependent on the density of proxy records available, but our uncertainty in the reconstruction increases as the number of proxy records decreases.

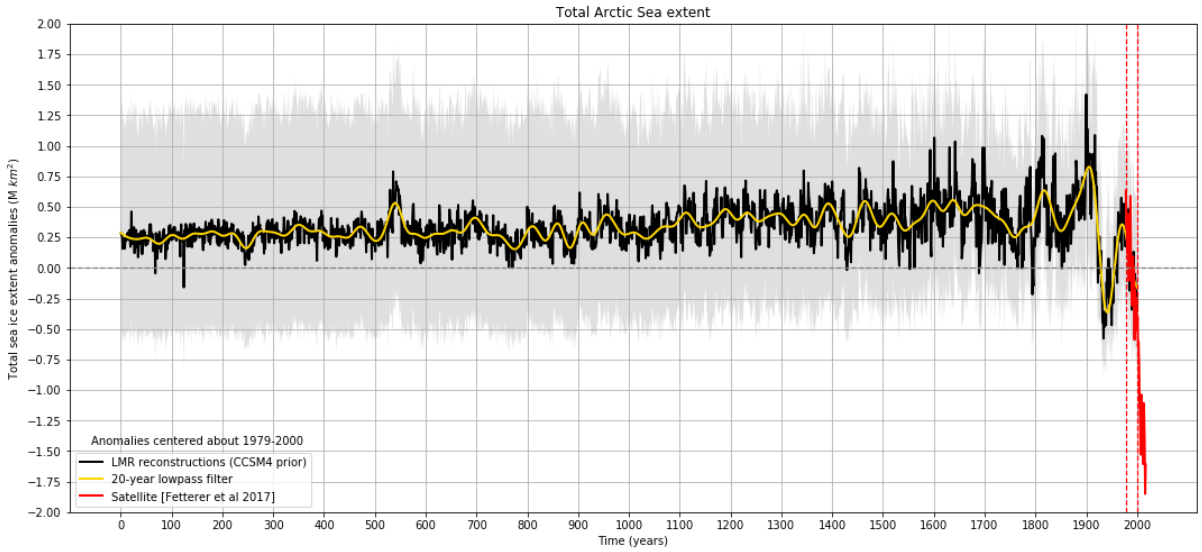

Figure 3.13: *A 2000-year total Arctic sea ice extent LMR reconstruction in black. The prior was drawn from the CCSM4 last millennium run and shown is the ensemble mean of 200 ensemble members for 5 Monte Carlo iterations. The shaded region indicates the 5th and 95th percentiles of the ensemble spread. The total Arctic sea ice extent derived from satellite observations (Fetterer et al., 2017) between the years 1979-2017 CE is shown in red. The vertical dashed red lines indicate the period of overlap between the two datasets (1979-2000 CE) and the period which all anomalies are centered about.*

Other notable features of this reconstruction include that Arctic sea ice extent was

steadily increasing between approximately 800 CE through 1900 CE. This is consistent with northern hemisphere millennial-scale cooling that has been documented in temperature records (Kaufman et al., 2009) and is also seen in the LMR temperature reconstructions. Also the large spike around 540 CE corresponds with a series of large volcanic eruptions documented in Sigl et al. (2015).

3.2.3 Changes to the distribution and trend of Arctic sea ice extent

Given this long sea ice reconstruction, scientific questions surrounding the natural variability of sea ice can be investigated. Here, we'll examine whether the current changes to Arctic sea ice extent observed in the satellite record are unprecedented in the last 1000 years. At 1000 CE the number of proxy records drops below 100, so the variance in the reconstruction becomes damped potentially artificially. For this reason, only the years 1000-2000 CE will be considered or emphasized for the later portion of this analysis.

Total Arctic sea ice extent

After around the year 2000 CE, the satellite data reaches total sea ice extent values that are lower than any other time in the 2000 year LMR reconstruction (see Figure 3.13). Furthermore, the later portion of the satellite data is well outside to the ensemble spread of the LMR reconstruction, which implies that the satellite observations are unprecedented.

The distribution of satellite data and the LMR reconstructions of total sea ice extent are examined, to further investigate whether recent observations of total sea ice extent are unprecedented relative to these longer sea ice reconstructions. Figure 3.14 shows the distribution of total Arctic sea ice extent anomalies from an LMR reconstruction (CCSM4 prior) between 1000-2000 CE in dark blue. The post-industrial period (1851-2000 CE) from the same reconstruction is shown in light blue to highlight which bins this time period occupies in the overall distribution. Note that the later portion of this reconstruction (light blue) occupies most of the low (and some of the high) portions of the distribution. This indicates

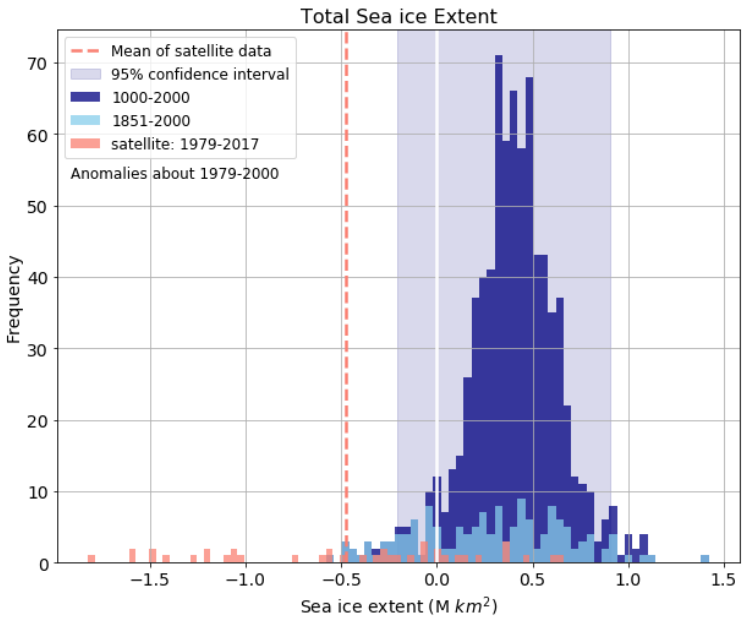

Figure 3.14: *Shown is the distribution of total Arctic sea ice extent values from an LMR reconstruction between 1000-2000 CE in dark blue, 1851-2000 CE in light blue and from satellite data between 1979-2017 in pink. The purple shaded box indicates the 95% confidence interval for the distribution from the LMR reconstruction between 1000-2000 CE. All values are anomalies centered about 1979-2000 CE, so the vertical white line indicates zero. The vertical dashed pink line indicates the mean of the satellite data.*

that most of the extremely low values in the last 1000 years occurred in the post-industrial period.

The pink values are the distribution of total Arctic sea ice extent derived from satellite observations between 1979-2017 CE. About half of the values in the satellite distribution overlap with values in the the LMR reconstructed distribution, but the mean is outside the 95% confidence interval of the reconstruction distribution, indicating that these two distributions are significantly different.

Based on Figure 3.13 and Figure 3.14 the total Arctic sea ice extent values observed in the satellite record have a significantly distribution that that in the LMR reconstructions over the last 1,000 years.

Trends in total Arctic sea ice extent

Figure 3.16 shows the distribution of trends in total Arctic sea ice extent derived from both LMR reconstructions and satellite observations. The distribution from LMR reconstructions (CCSM4 prior) between 1000-2000 CE are shown in dark blue and the period between 1851-2000 CE is highlighted in light blue. The distribution derived from satellite data (1979-2017 CE) is shown in pink. These trends were derived by taking the 10, 20, and 30-year trend at each time step in each dataset, thus these values are not independent.

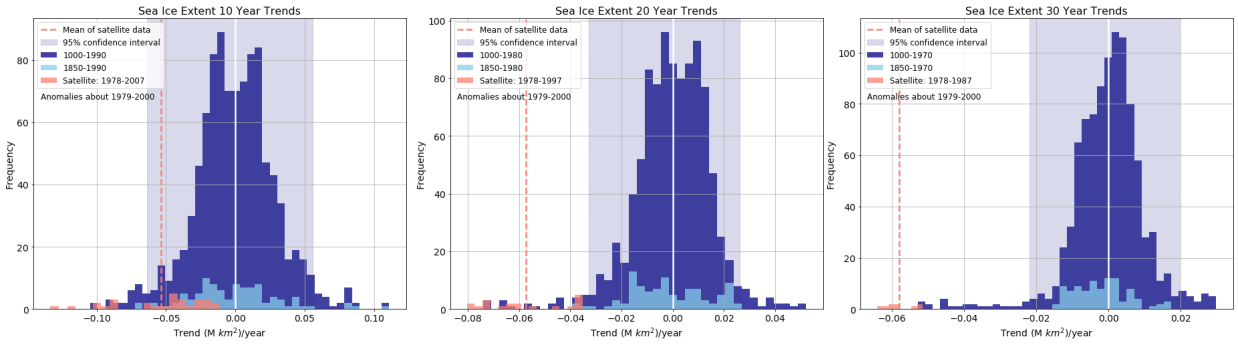

a) b) c)

Figure 3.16: *Shown are the distribution of 10 (a), 20 (b), and 30 (c) year trends in total arctic sea ice extent. The trends from an LMR reconstruction (CCSM4 prior) between 1000-2000 CE are shown in dark blue and the period of 1851-2000 CE is highlighted in light blue. The trends observed in satellite data between 1979-2017 CE are shown in pink. The shaded purple box indicates the 95% confidence interval of the dark blue distribution and the vertical white line indicates zero trend. The vertical dashed pink line indicates the mean trend observed in the satellite data.*

The distribution of trends from the LMR reconstructions transitions from being centered around zero for 10-year trends to skewed to the left for 30-year trends. Unlike with the total Arctic sea ice values, the extreme negative trends did not mostly occur in the post-industrial period (light blue distribution in Figure 3.16). Recall that in Section 3.2.1, we found that the reconstructions underestimate the trends in the satellite era. For 10-year trends, the satellite data mostly overlaps with the reconstructed trends and the satellite mean falls within the 95% confidence interval of the reconstructed distribution. For 20 and 30-year trends, the mean of the satellite data is well outside the 95% confidence interval of the reconstructed

distribution indicating that these trends in the satellite data are unprecedented (particularly for 30-year trends).

Based on this analysis both the trends and values of total Arctic sea ice extent observed in the satellite era are unprecedented when compared to the LMR reconstructed values over the last 1000 years.

3.2.4 Sea ice response to volcanic eruptions

There are many drivers of natural sea ice variability. Some of the major factors include: the Arctic Oscillation, Atlantic Multidecadal Variability, and volcanic eruptions. Ultimately, we would like to investigate the affect of all of these and factors on sea ice variability in LMR reconstructions, but will leave much of this to future work. Here we'll investigate how sea ice responds to volcanic eruptions in the LMR reconstructions.

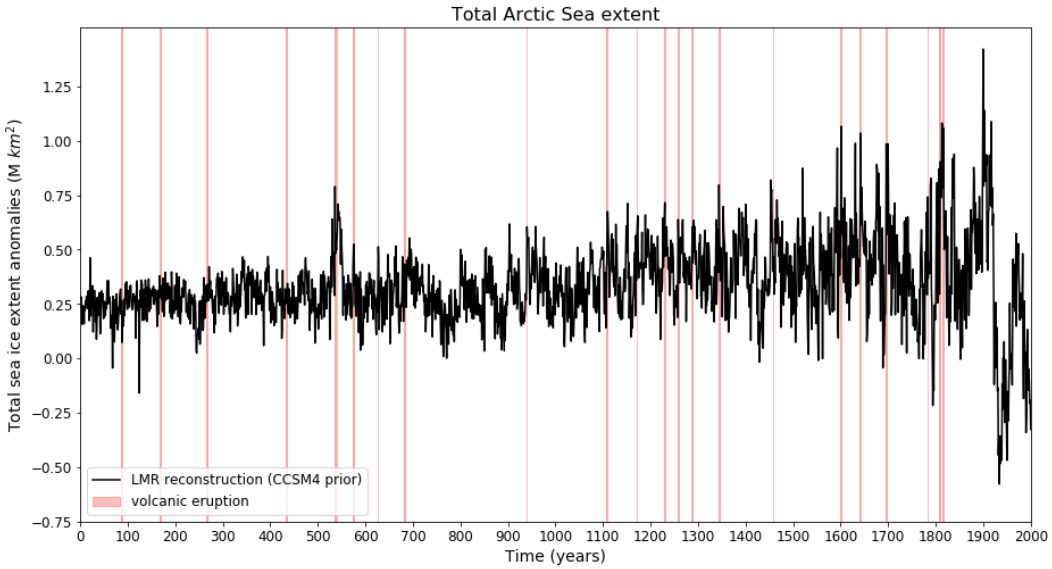

Figure 3.17: *In black is an LMR reconstruction (CCSM4 prior) of total Arctic sea ice extent. Shown in the mean of 200 ensemble member from 5 monte carlo iterations. The red vertical lines indicate the year of the 23 largest pre-industrial volcanic eruptions (based on global radiative forcing) from Sigl et al. (2015).*

To examine this, the sea ice extent before and after the 23 largest pre-industrial eruptions (taken from Sigl et al. (2015)) were examined. Figure 3.17, shows the LMR reconstructed

total annual Arctic sea ice extent with the years of these large volcanic eruptions shown as vertical red lines. Looking at this figure, many of the years with a large volcanic eruption correspond with a spike in sea ice extent, but not all of them. To investigate this further, the 5 years before and 15 years after each of these eruptions were selected and the resulting composite is shown in Figure 3.18. The total Arctic sea ice extent about each of these eruptions is shown in a light blue line. The red vertical line indicates the year of the eruption. The composite mean is shown in a darker blue bold line and all anomalies are centered about the 5 years preceding each eruption. Figure 3.18 indicates that there is elevated Arctic sea ice extent for about 10 years after a volcanic eruption though the values are only significant for one year following an eruptions.

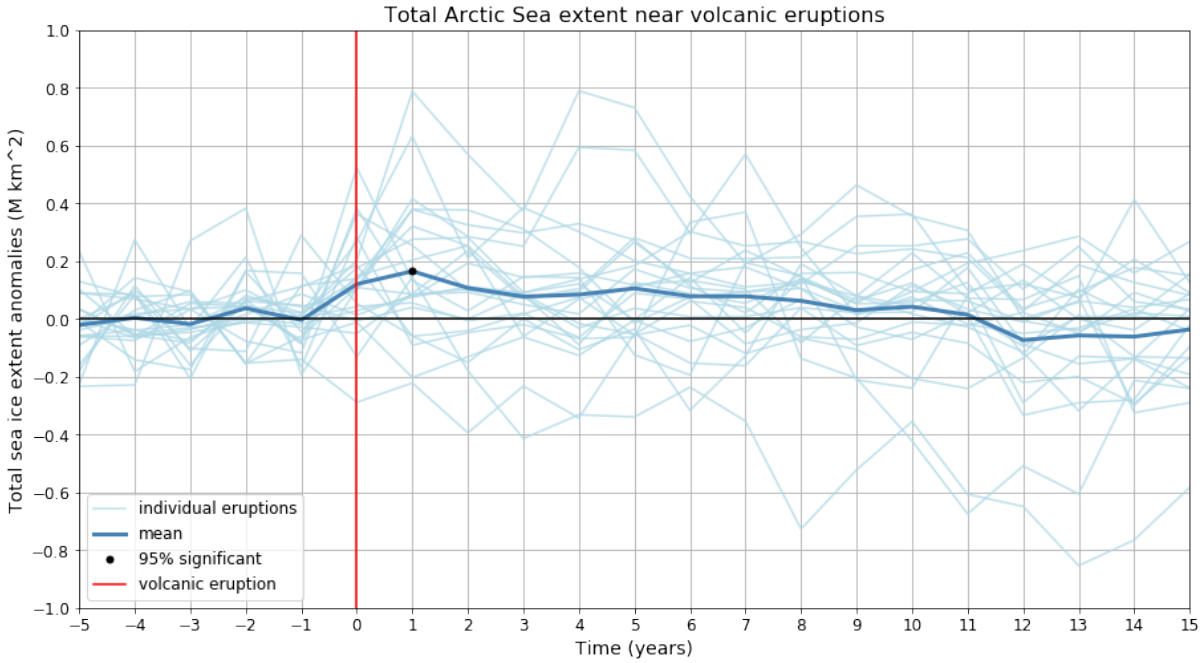

Figure 3.18: *Composites total Arctic sea ice extent for the 5 years before and 15 years after major volcanic eruptions.*

There is a slight increase in areal coverage of sea ice after large volcanic eruptions, but the affect is generally small in these LMR reconstructions and only significant for one year following the largest eruptions.

3.3 Sensitivity Testing

Various parameters in the LMR framework influence the resulting sea ice reconstructions including: the proxy record type, proxy record locations, prior, number of ensemble members, localization length scale, and proxy system model used. Here, the influence of the proxy record location, and sensitivity of the results to the prior and number of ensemble members used are investigated.

3.3.1 Sensitivity to proxies

Two major aspects of proxy records could influence these reconstructions: proxy location and type. Here we investigate which proxy region has the most influence on LMR sea ice reconstructions. To investigate this, various reconstructions were produced using proxy records from specified regions. For these experiments, the pages2Kv1 network was used as described in Section 2.2.1 (see Figure 2.3) because the proxy records are automatically sorted by region in this database. It is left to future work to repeat these experiments with the LMRdbv1 proxy network. These experiments were performed using a localization length scale of 25,000 km (like all other reconstructions in this study), so by design a proxy cannot have influence a region beyond about a hemisphere away. The expectation is that Arctic proxies (north of 60°N) will have the most influence on LMR Arctic sea ice reconstructions.

Figure 3.19 shows the ensemble mean total Arctic sea ice extent from four different reconstructions which used CCSM4 last millennium run as a prior and 10 monte carlo iterations with 200 ensemble members each. For each of these reconstructions, different proxy regions were used: global (black), only Arctic (blue), only northern hemisphere (purple), and only southern hemisphere (grey). The Pages2kv1 database includes 462 proxies, but only 346 proxies are used in each reconstruction (25% are withheld for verification purposes). 305 of these proxies are in the northern hemisphere, 41 are in the southern hemisphere and 20 are in the Arctic.

The reconstruction using only Arctic proxies in Figure 3.19 shows slightly damped vari-

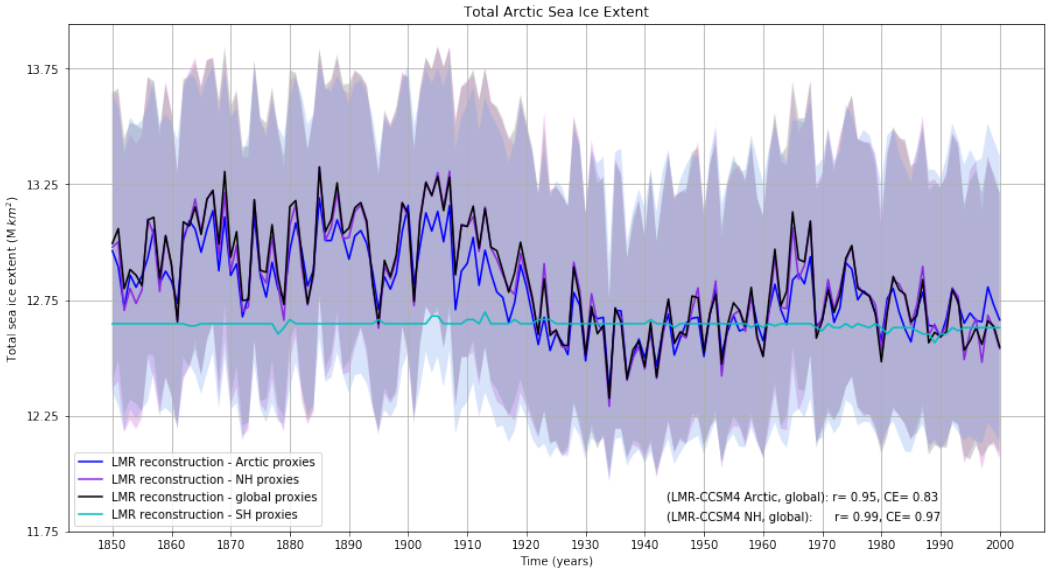

Figure 3.19: *LMR reconstructions using CCSM4 last millennium run and the Pages2k version 1 (Pages2k Consortium, 2013) global (black), only Arctic (blue), and only northern hemisphere (purple) proxies.*

ability when compared to the global proxy reconstruction because there were considerably fewer proxies assimilated. However, using only Arctic proxies does capture a majority of the variability observed in the global proxy reconstruction with a correlation coefficient of 0.95 and coefficient of efficiency of 0.83. Using proxy records only in the northern hemisphere captures nearly all of the signal in the global proxy reconstruction with a correlation coefficient of 0.99 and coefficient of efficiency of 0.97. The reconstruction using only southern hemisphere proxy records is nearly a flat line due to the localization length scale used (no proxy influence from the southern hemisphere). Therefore, Arctic proxies have a majority of the influence on the LMR sea ice reconstructions, but some information is added from proxies in the northern hemisphere.

3.3.2 Sensitivity to priors

As shown in the imperfect pseudo proxy results, these reconstructions are dependent on the model prior used. However, the pan-Arctic indices of sea ice extent reconstructed using four different priors (see Figure 3.10) all show similar overall sea ice extent and variance through

time. The total quantity of sea ice is similar when different model priors are used, but their spatial patterns can deviate. This is, as mentioned in section 3.1.2, most likely due to differences in the spatial covariance patterns between temperature and sea ice in different models. Here we investigate these differences.

To begin, the covariance between temperature at one grid cell and northern hemisphere sea ice everywhere was calculated using the full 1000 year run. For these experiments only northern hemisphere values were considered, because as shown in Section 3.3.2 the southern hemisphere has no influence on the Arctic sea ice reconstructions. This was repeated for every northern hemisphere temperature grid cell for each of the four last millennium prior runs (CCSM4, MPI, GISS, and Hadcm3). Then the correlation coefficient and CE was calculated between the spatial covariance pattern associated with each temperature grid cells between different models. For example, the spatial covariance was calculated for the temperature at a point in Iceland with Arctic sea ice everywhere in CCSM4 last millennium run. The correlation coefficient and CE was then calculated between this spatial covariance pattern and the same in the MPI past 1000 run. The correlation coefficient and CE value at each temperature grid cell is plotted on a map in Figure 3.20 (see page 46).

Generally, the maps in Figure 3.20 indicate where the covariance between temperature and sea ice agree and disagree across different models. Depending on the error in the prior and proxy data, proxies in regions where these covariances disagree may be treated differently when priors are drawn for the different models. More specifically, regions that show a high correlation coefficient reflect regions where the the covariance of temperature in that region and Arctic sea ice overlap between the models. Regions where there are high CE values reflect regions where the magnitude and mean of the covariance of temperature in that region and Arctic sea ice agree across the models. Regions where there is negative CE values reflect regions where the variance and/or mean of the covariance patterns differ.

There this strong correlation between the spatial covariance patterns in different priors with correlation coefficients exceeding 0.5 in most regions. Most regions exhibit positive CE values with some patches of negative CE values generally in the North Atlantic and over

China and Russia depending on the two models being compared. The best overall agreement is between CCSM4 and MPI (Figure 3.20a).

3.3.3 Number of ensemble members

The LMR framework uses an ensemble drawn from last millennium model output to estimate the covariance between temperature and sea ice. The covariance in the entire model run is assumed to be the most robust, therefore, it is important to ensure that the ensemble size used is large enough to represent the entire model run.

To test this, we assume that the covariance of temperature at a proxy location (or the grid cell closest to that location) and Arctic sea ice in the entire 1000 year model run is our best estimate of the covariance between those two quantities (as opposed to some subset of years). The covariance of the full 1000 year run is then calculated, which we'll call the *ideal* spatial covariance pattern. Then, an ensemble size ranging from 1 to 1000 members of random years is drawn from the model output and the spatial covariance pattern is calculated between temperature at a grid cell and northern hemisphere sea ice across the ensemble. The coefficient of efficiency is then calculated between the *ideal* spatial covariance pattern and the spatial covariance pattern for each ensemble size. This results in a coefficient of efficiency for each ensemble size for each temperature grid cell. An example of this for one location in Svalbard is shown in Figure 3.21. As the ensemble size approaches 1000 the coefficient of efficiency converges to 1.0 because the random sample becomes equivalent to the *ideal* spatial covariance pattern.

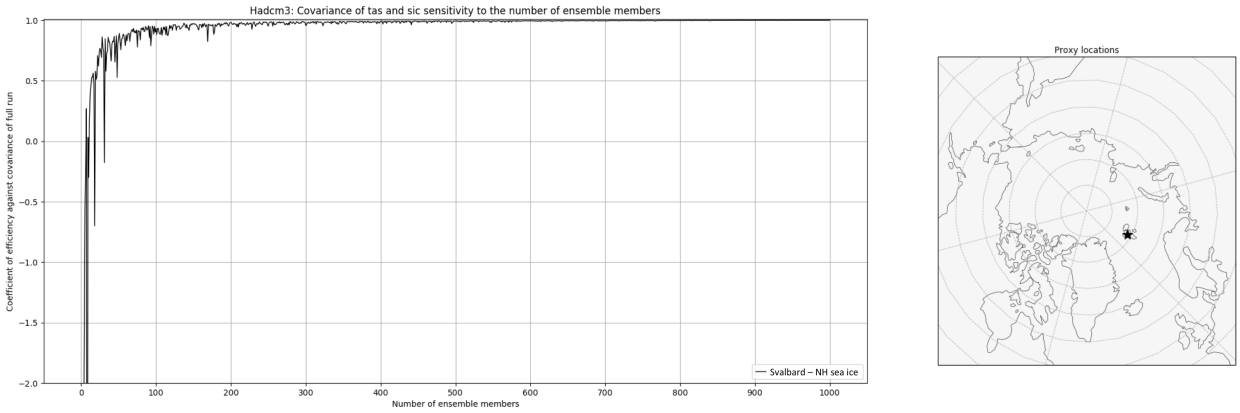

Figure 3.21: *Shown in the convergence of the coefficient of efficiency between surface temperature at a point in Iceland (shown as a black star on the map), and northern hemisphere sea ice concentration for varying number of ensemble members and the same covariance from the full 1000 years of the prior.*

For this point in Svalvard (shown in Figure 3.21), covariance pattern converges for small ensemble sizes (less than 100 ensemble members), but the same is not necessarily true for all proxy locations. To show this, this process was repeated for every temperature grid cell for three different ensemble sizes. Running a reconstruction with more than 300 ensemble members is impractical due to the computational time and storage space necessary; Therefore, for these global plots of the CE values were calculated for only 100, 200, and 300 ensemble members for each model prior (see Figure 3.22). To be explicit, the color of a grid cell over Svalbard in Figure 3.22 are the points on the curve corresponding to 100, 200, and 300 ensemble members in Figure 3.21. The results shown in Figure 3.22 are the average of 10 iterations of this process and the stippling shows regions where the coefficient of efficiency exceeds 0.9.

Large areas of negative CE values in the northern hemisphere in Figure 3.22, indicate that 100 ensemble members might not be sufficient for sea ice LMR reconstructions. The spatial distribution of the CE values looks different for different models. Regions with negative CE values are regions where the covariance of temperature at those points and northern hemisphere sea ice are not consistent with the *ideal* spatial covariance pattern. Some of these regions are expected to have negative CE values. For example, the covariance between air temperature over the southern ocean and northern hemisphere sea ice is expected to be

small and noisy, so negative CE values over the southern ocean are expected. Furthermore, since a localization length scale of 25,000 km is used, northern hemisphere proxies have the most influence Arctic reconstructions (as shown in Section 3.4.1), so are most concerned with the northern hemispheres in Figure 3.22.

The concentration of negative CE values decreases as the ensemble size increases. In particular, much of the negative CE values in the northern hemisphere diminish when 200 ensemble members are used, and the Arctic region shows high positive CE values with a significant portions of the region showing CE values greater than 0.9 shown with stippling (particularly for CCSM4 and GISS). Therefore, 200 ensemble members were used in these reconstructions due to the balance between the convergence of these covariance patterns and the storage space required to hold large ensemble sizes.

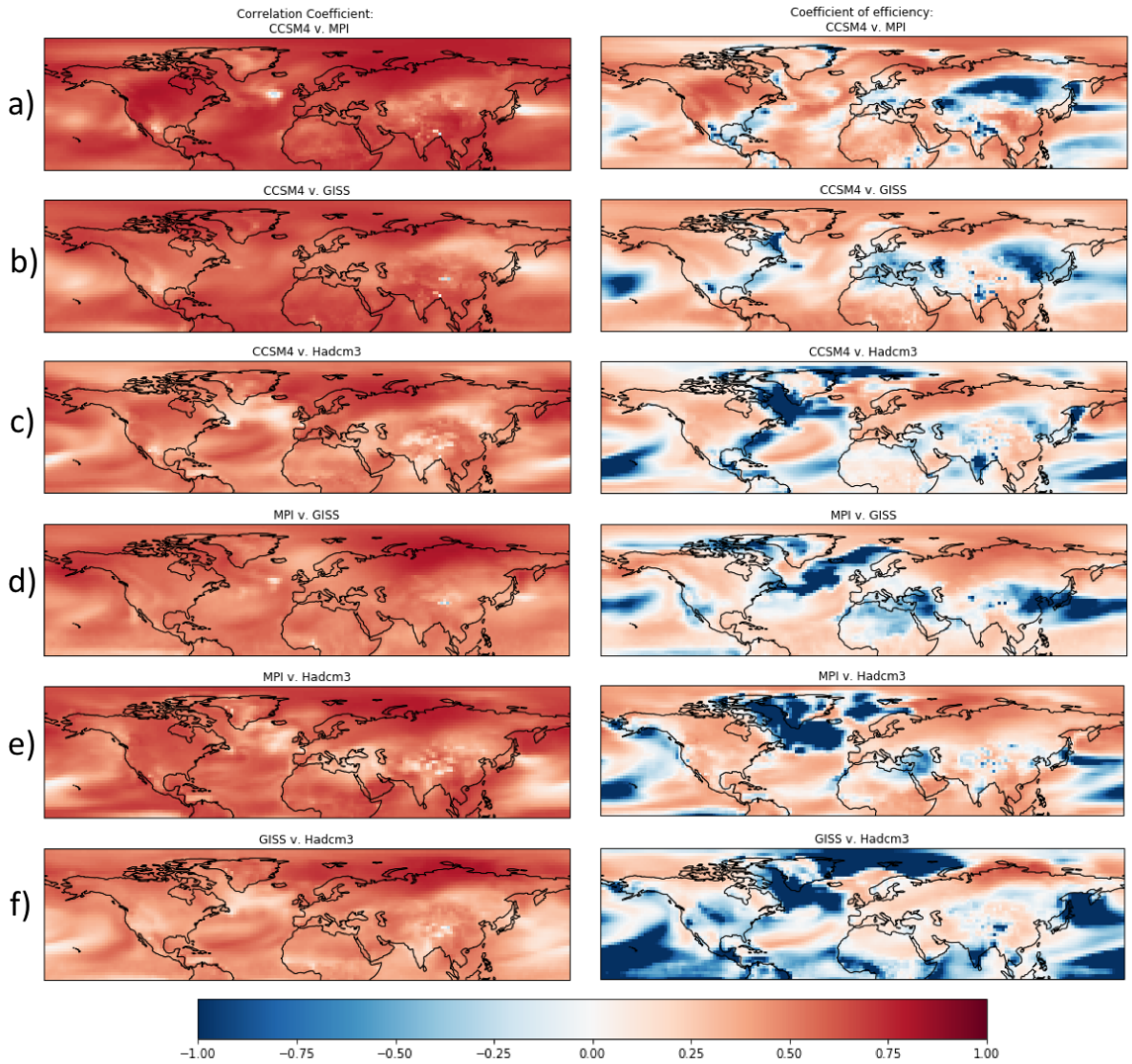

Figure 3.20: *The covariance of temperature at each northern hemisphere grid cell and sea ice at all northern hemisphere grid cells was calculated for each prior model last millennium run (CCSM4, MPI, GISS, Hadcm3). Shown is the correlation coefficient and coefficient of efficiency calculated for that spatial pattern between all the models.*

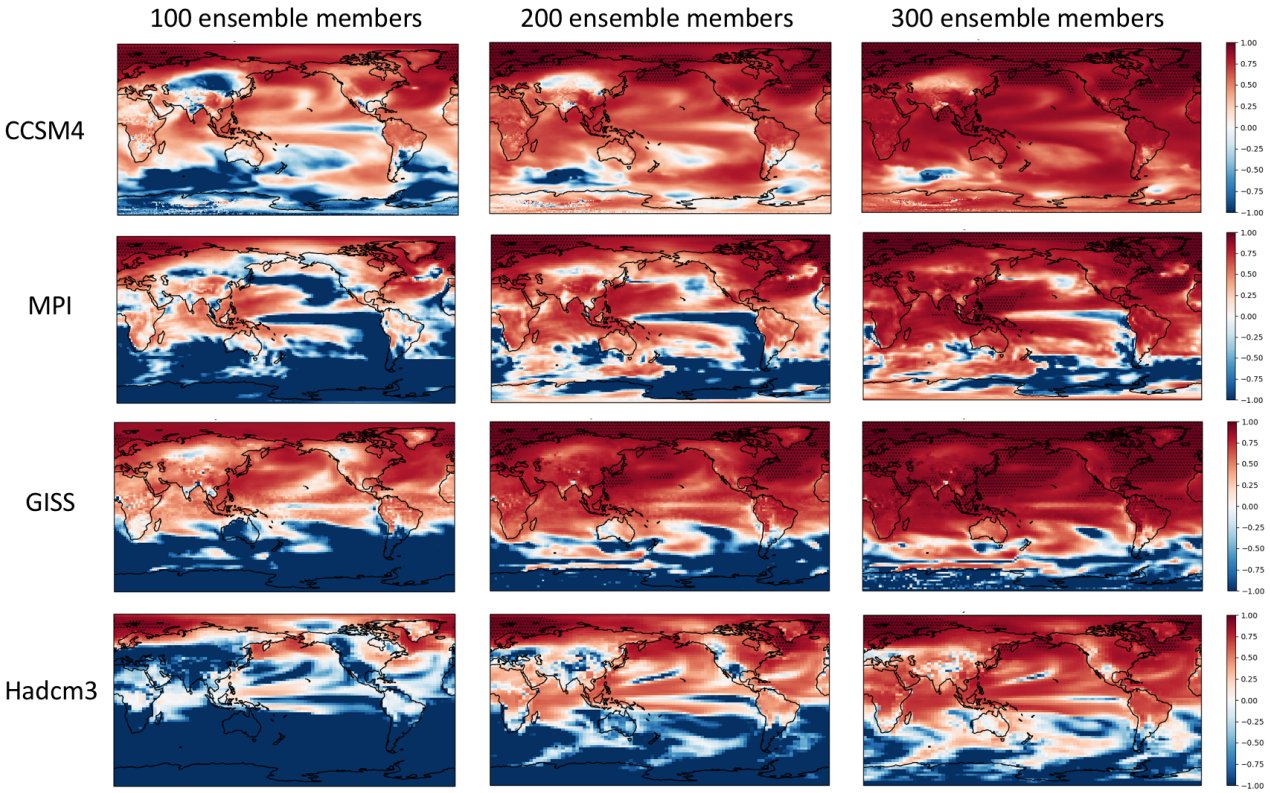

Figure 3.22: *Shown in color are the coefficient of efficiency between the covariance of surface temperature at each grid cell and northern hemisphere sea ice concentration for the entire 1000 year prior and for a random sample of 100, 200, and 300 ensemble members (random years from the 1000 year prior). Each figure is the mean of 10 iterations of the random draw of ensemble members.*

Chapter 4
CONCLUSIONS AND DISCUSSION

Pseudo Proxy Experiments

Perfect and imperfect pseudo proxy experiments were performed to evaluate the performance of LMR Arctic sea ice reconstructions. Overall, both the perfect and imperfect pseudo proxy experiments show good performance in reconstructing total annual Arctic sea ice extent and annual Arctic sea ice concentration at each grid cell. The imperfect pseudo proxy experiments showed weaker performance than the perfect model experiments as expected. This indicates that the prior has some influence on the reconstruction likely through the inherited covariance structures from the prior ensemble between surface air temperature and sea ice.

Real Proxy Experiments

Real proxy records were assimilated into prior ensembles drawn from four different models (CCSM4, MPI, GISS, and Hadcm3) resulting in 2000 year annual Arctic sea ice reconstructions. These reconstructions were compared with satellite data, and other longer records and reconstructions. All four reconstructions show good comparison with satellite data with correlation coefficients ranging between 0.54 (Hadcm3 prior) and 0.84 (GISS prior) and CE values ranging bewteen 0.27 (Hadcm3 prior) and 0.66 (GISS prior), and the four reconstructions agree with one another as well. When compared to a longer observationally based record from Walsh et al. (2017), the LMR reconstructions show larger and longer lasting sea ice lows between 1920-1970 CE with values similar to those observed in the 1990s. This decline is in response to early 20th century warming, which is well represented in the LMR temperature reconstructions when compared to observations. The LMR reconstructions were also compared to the summer sea ice extent reconstructions from Kinnard et al. (2011). Qual-

itative comparisons were difficult due to damped variability in the LMR reconstructions on longer timescales, which is thought to be due to some of the proxy records used and needs to be investigated further.

The longer sea ice reconstructions were then used to investigate the significance of the Arctic sea ice declines observed in the satellite era and the Arctic sea ice response to volcanic eruptions. The distribution of total Arctic sea ice extent values and trends was used to determine that the Arctic sea ice conditions in the satellite record are outside the distribution of Arctic sea ice extent values and trend the last 1000 years of the LMR reconstruction. Then a composite of the sea ice conditions before and after the 23 largest volcanic eruptions in the pre-industrial period was examined. These results shows that, on average, Arctic sea ice extent does increase following an eruption, but that increase is only statistically significant one year after the eruption.

Sensitivity Testing

The effect of the proxy locations, model priors, and number of ensemble members used on the LMR sea ice reconstructions was examined. Arctic proxy records (above 60°N) were found to explain most of the variance in the global proxy reconstructions. More influence from northern hemisphere proxies was expected given that a localization length scale of 25,000 km was used (about a hemisphere of influence). The covariance between surface air temperature and Arctic sea ice is compared across four last millennium model runs (CCSM4, MPI, GISS and Hadcm3) to investigate how different priors may affect the reconstructions. The covariance structure in all models is similar with positive correlation coefficients everywhere. There are some regions that show a negative coefficient of efficiency indicating that the mean and/or variance differs across models in central Russia and China, the north Atlantic and central Pacific. Proxies in these locations will be handled differently by the Kalman filter when different model priors are used. Finally, different prior ensemble sizes were tested to verify that the ensemble adequately represented the covariance between surface air temperature and Arctic sea ice. 200 ensemble members was determined to be ample, as it represents the

full 1000-year run in the northern hemisphere well and doesn't require excessive amounts of data storage.

Future work

There are various aspects of these experiments that could be improved upon. First I would like to further investigate the response of sea ice to early 20th century warming. This will involve investigating the differences between the Walsh et al. (2017) dataset and the LMR reconstructions. Other things I would like to investigate include looking at total sea ice volume indices, reconstructing seasonal sea ice and incorporating a linear inverse model to do online data assimilation.

BIBLIOGRAPHY

Anderson, D., Tardif, R., Horlick, K., Erb, M., Hakim, G., Noone, D., Perkins, W., and Steig, E. (2019). Additions to the Last Millennium Reanalysis multi-proxy database. *Data Science Journal*, 18(1):2.

Armour, K. C. and I. Eisenman and E. Blanchard−Wrigglesworth and K. E. McCusker and C. M. Bitz (2011). The reversibility of sea ice loss in a state of the art climate model. *Geophysical Research Letters*, 38.

Belt, S. T. and Müller, J. (2013). The arctic sea ice biomarker IP_{25}: a review of current understanding, recommendations for future research and applications in palaeo sea ice reconstructions. *Quatenary Science Reviews*, 79:9–25.

Belt, S. T., , G. M., Rowland, S. J., Poulin, M., Michel, C., and LeBlanc, B. (2007). A novel chemical fossil of palaeo sea ice: IP_{25}. *Organic Geochemistry*, 38:16–27.

Compo, G. P., Whitaker, J. S., Sardeshmukh, P. D., Matsui, N., Allan, R. J., Yin, X., B. E. Gleason, J., Vose, R. S., Rutledge, G., Bessemoulin, P., Bronnimann, S., Brunet, M., Crouthamel, R. I., Grant, A. N., Groisman, P. Y., Jones, P. D., Kruk, M. C., Kruger, A. C., Marshall, G. J., Maugeri, M., Mok, H. Y., Nordli, Ø., Ross, T. F., Trigo, R. M., Wang, X. L., Woodruff, S. D., and Worleyu, S. J. (2011). Review article the twentieth century reanalysis project. *Quarterly Journal of the Royal Meteorological Society*, 137:1–28.

Cook, E. R., Seager, R., Kushnir, Y., Briffa, K. R., Büntgen, U., Frank, D., Krusic, P. J., Tegel, W., van der Schrier, G., Andreu-Hayles, L., Baillie, M., Baittinger, C., Bleicher, N., Bonde, N., Brown, D., Carrer, M., Cooper, R., Čufar, K., Dittmar, C., Esper, J.,

Griggs, C., Gunnarson, B., Günther, B., Gutierrez, E., Haneca, K., Helama, S., Herzig, F., Heussner, K.-U., Hofmann, J., Janda, P., Kontic, R., Köse, N., Kyncl, T., Levanič, T., Linderholm, H., Manning, S., Melvin, T. M., Miles, D., Neuwirth, B., Nicolussi, K., Nola, P., Panayotov, M., Popa, I., Rothe, A., Seftigen, K., Seim, A., Svarva, H., Svoboda, M., Thun, T., Timonen, M., Touchan, R., Trotsiuk, V., Trouet, V., Walder, F., Ważny, T., Wilson, R., and Zang, C. (2015). Old world megadroughts and pluvials during the common era. *Science*, 1(10).

Dyke, A. S., Hooper, J., and Savelle, J. M. (1996). A history of sea ice in the canadian arctic archipelago based on postglacial remains of the Bowhead whale (Balaena mysticetus). *Arctic*, 49:235–255.

England, J. H., Lakeman, T. R., Lemmen, D. S., Bednarski, J. M., Stewart, T. G., and Evans, D. J. A. (2008). A millennial-scale record of Arctic ocean sea ice variability and the demise of the Ellesmere Island ice shelves. *Geophysical Research Letters*, 35.

Evensen, G. (2003). The ensemble Kalman filter: Theoretical formulation and practical implementation. *Ocean Dynamics*, 53:343–367.

Fetterer, F., Knowles, K., Meier, W. N., Savoie, M., and Windnagel, A. K. (updated daily, 2017). Sea ice index, version 3. *Boulder, Colorado USA. NSIDC: National Snow and Ice Data Center.*

Gaspari, G. and Cohn, S. E. (1999). Construction of correlation functions in two and three dimensions. *Quart. J. Roy. Meteor. Soc*, 125:723–757.

Goosse, H., Roche, D., Mairesse, A., and Berger, M. (2013). Modeling past sea ice changes. *Quaternary Sciences Reviews*, 79:191–206.

Hakim, G., Emile-Geay, J., Steig, E., Noone, D., Anderson, D., Tardif, R., Steiger, N., and W. Perkins 121, .-. (2016). The last millennium climate reanalysis project: Framework and first results. *Journal of Geophysical Research: Atmospheres*, 121:6745–6764.

Hamill, T. M., Whitaker, J. S., and Snyder, C. (2001). Distance-dependent filtering of background error covariance estimates in an ensemble Kalman filter. *American Meteorological Society Monthly Weather Review*, 129:2776–2790.

Hansen, J., Ruedy, R., Sato, M., and Lo, K. (2010). Global surface temperature change. *Review of Geophysics*, 48.

Holton, J. R. and Hakim, G. J. (2013). *An Introduction to Dynamic Meteorology*. Academic Press, fifth edition.

Jones, P. D. and Moberg, A. (2003). Hemispheric and large-scale surface air temperature variations: An extensive revision and an update to 2001. *Journal of Climate*, 16:206–223.

Kaufman, D. S., Schneider, D. P., McKay, N. P., Ammann, C. M., Bradley, R. S., Briffa, K. R., Miller, G. H., Otto-Bliesner, B. L., Overpeck, J. T., Vinther, B. M., and 2k Project Members, A. L. (2009). Recent warming reverses long-term Arctic cooling. *Science*, 325:1236–1239.

Kay, J. E., Holland, M. M., and Jahn, A. (2011). Interannual to multidecadal Arctic sea ice extent trends in a warming world. *Geophysical Research Letters*, 38.

Kinnard, C., Zdanowicz, C. M., Fisher, D. A., Isaksson, E., de Vernal, A., and Thompson, L. G. (2011). Reconstructed changes in Arctic sea ice over the past 1,450 years. *Nature Letters*, 479:509–513.

Klein, F., Goose, H., Mairesse, A., and de Vernal, A. (2014). Model-data comparison and data assimilation of mid-Holocene Arctic sea ice concentration. *Climate of the Past*, 10:1145–1163.

Landrum, L., Otto-Bliesner, B. L., Wahl, E. R., Conley, A., Lawrence, P. J., Rosenbloom, N., and Teng, H. (2013). Last millennium climate and its variability in ccsm4. *Journal of Climate*, 26:1085–1111.

Mahlstein, I. and Knutti, R. (2012). September Arctic sea ice predicted to disappear near 2 c global warming above present. *Journal of Geophysical Research*, 117.

Maslanik, J. A., Fowler, C., Stroeve, J., Drobot, S., Zwally, J., Yi, D., and Emery, W. (2007). A younger, thinner Arctic ice cover: Increased potential for rapid, extensive sea-ice loss. *Geophysical Research Letters*, 34.

Massé, G., Rowland, S. J., Sicre, M.-A., Jacob, J., Jansen, E., and Belt, S. T. (2008). Abrupt climate changes for Iceland during the last millennium: Evidence from high resolution sea ice reconstructions. *Earth and Planetary Science Letters*, 269:565–569.

Meier, W. N., Hovelsrud, G. K., van Oort, B. E., Key, J. R., Kovacs, K. M., Michel, C., Haas, C., Granskog, M. A., Gerland, S., Perovich, D. K., Makshtas, A., and Reist, J. D. (2014). Arctic sea ice in transformation: A review of recent observed changes and impacts on biology and human activity. *Reviews of Geophysics*, 51:185–217.

Notz, D. (2015). How well must climate models agree with observations? *Philosophical Transactions Royal Society*, 373.

Notz, D. and Marotzke, J. (2012). Observations reveal external driver for Arctic sea-ice retreat. *Geophysical Research Letters*, 39.

Notz, D. and Stroeve, J. (2016). Observed Arctic sea-ice loss directly follows anthropogenic co2 emission. *Science*, 354(6313):747–750.

Oke, P. R., Allen, J. S., Miller, R. N., Egbert, G. D., and Kosro, P. M. (2002). Assimilation of surface velocity data into a primitive equation coastal ocean model. *Journal of Geophysical Research*, 107(C9).

Overland, J. E., Wood, K. R., and Wang, M. (2011). Warm Arctic cold continents: climate impacts of the newly open Arctic Sea. *Polar Research*, 30.

Pages2k Consortium (2013). Continental-scale temperature variability during the past two millennia. *Nature Geosciences*, 6:339–345.

Pages2k Consortium (2017). Data descriptor: A global multiproxy database for temperature reconstructions of the Common Era. *Nature: Scientific Data*.

Polyak, L., Alley, R. B., Andrews, J. T., Brigham-Grette, J., Cronin, T. M., Darby, D. A., Dyke, A. S., Fitzpatrick, J. J., Funder, S., Holland, M., Jennings, A. E., Miller, G. H., O'Regan, M., Savelle, J., Serreze, M., John, K. S., White, J. W., and Wolff, E. (2010). History of sea ice in the Arctic. *Quatenary Science Reviews*, 29(15-16):1757–1778.

Polyakov, I. V., Alekseev, G. V., Bekryev, R. V., Bhatt, U. S., Colony, R., Johnson, M. A., Karklin, V. P., Walsh, D., and Yulin, A. V. (2003). Long-term ice variability in Arctic marginal seas. *Journal of Climate*, 16:2078–2085.

Renssen, H., Goosse, H., Fichefet, T., Brovkin, V., Driesschaert, E., and Wolk, F. (2005). Simulating the Holocene climate evolution at northern high latitudes using a coupled atmosphere-sea ice-ocean-vegetation model. *Climate Dynamics*, 24:23–43.

Rosenblum, E. and Eisenman, I. (2017). Sea ice trends in climate models only accurate in runs with biased global warming. *Journal of Climate*, 30:6265–6278.

Schmidt, G. A., Jungclaus, J. H., Ammann, C. M., Bard, E., Braconnot, P., Crowley, T. J., Delaygue, G., Joos, F., Krivova, N. A., Muscheler, R., Otto-Bliesner, B. L., Pongratz, J., Shindell, D. T., Solanki, S. K., Steinhilber, F., and Vieira, L. E. A. (2011). Climate forcing reconstructions for use in PMIP simulations of the last millennium (v1.0). *Geoscientific Model Development*, 4:33–45.

Schneider, U., Becker, A., Finger, P., Meyer-Christoffer, A., Ziese, M., and Rudolf, B. (2014). GPCC's new land surface precipitation climatology based on quality-controlled in situ data and its role in quantifying the global water cycle. *Theoretical and Applied Climatology*, 115:15–40.

Serreze, M. C., Holland, M. M., and Stroeve, J. (2007). Perspectives on the Arctic's shrinking sea ice cover. *Science*, 315(5818):1533–1536.

Sigl, M., Winstrup, M., McConnell, J. R., Welten, K. C., Plunkett, G., Ludlow, F., ntgen, U. B., Caffee, M., Chellman, N., Dahl-Jensen, D., Fischer, H., Kipfstuhl, S., Kostick, C., Maselli, O. J., Mekhaldi, F., Mulvaney, R., Muscheler, R., Pasteris, D. R., Pilcher, J. R., Salzer, M., pbach, S. S., Steffensen, J. P., Vinther, B. M., and Woodruff, T. E. (2015). Timing and climate forcing of volcanic eruptions for the past 2,500 years. *Nature*, 523.

Singh, H. K. A., Hakim, G. J., Tardif, R., Emile-Geay, J., , and Noone, D. C. (2018). Insights into Atlantic multidecadal variability using the Last Millennium Reanalysis framework. *Climate of the Past*, 14:157–174.

Steiger, N. J., Hakim, G. J., Steig, E. J., Battisti, D. S., and Roe, G. H. (2014). Assimilation of time-averaged pseudoproxies for climate reconstruction. *Journal of Climate*, 27:426–441.

Stroeve, J., Hollan, M., Meier, W., Scambos, T., and Serreze, M. (2007). Arctic sea ice decline: Faster than forecast. *Geophysical Research Letters*, 34(9).

Tardif, R., Hakim, G. J., Perkins, W. A., Horlick, K. A., Erb, M. P., Emile-Geay, J., Anderson, D. M., Steig, E. J., and Noone, D. (2019). Last Millennium Reanalysis with an expanded proxy database and seasonal proxy modeling. *Climate of the Past*.

Walsh, J. E., Fetterer, F., Stewart, J. S., and Chapman, W. L. (2017). A database for depicting Arctic sea ice variations back to 1850. *Geophysical Review*, 107(1):89–107.

Whitaker, J. and Hamill, T. (2002). Ensemble data assimilation without perturbed observations. *AMS Monthly Weather Review*, 130:1913–1924.

Yamanouchi, T. (2011). Early 20th century warming in the Arctic: A review. *Polar Science*, 5:53–71.

VITA

Katie Brennan is a graduate student in the department of Atmospheric Sciences. She welcomes your comments to mkb22@uw.edu.